J. Fluid Mech. (1995), *vol.* 286, *pp.* 327–357

Linear potential theory of steady internal supersonic flow with quasi-cylindrical geometry. Part 2. Free jet flow

By ANDREAS DILLMANN

Deutsche Forschungsanstalt für Luft- und Raumfahrt, Bunsenstraße 10, D-37073 Göttingen, Germany

(Received 17 August 1994)

By extending the methods of Part 1, the general problem of steady cylindrical supersonic free jet flow is treated in a similar manner to the flow in quasi-cylindrical ducts. It is shown that the presence of a finite pressure jump at the nozzle lip gives rise to a periodic singularity pattern in the flow field. Basic examples of free jet flows are discussed, and for the case of a nearly ideally expanded axisymmetric jet, theoretical Mach–Zehnder interferograms are calculated by analytical integration of the density field. Excellent agreement with experiment proves the validity of linear theory even close to the singularities and far downstream of the nozzle orifice. Furthermore, it is shown that Pack's formula for the wavelength of the shock cell structure is inconsistent; the correct formula is derived and excellent agreement with Emden's empirical fit is found.

1 Introduction

Like the problem of supersonic flow in quasi-cylindrical ducts treated in Part 1 (Dillmann 1994*a*), the closely related phenomenon of cylindrical supersonic free jet flow has considerable practical impact. Important fields of application are found in aeroacoustics, where several theoretical models of noise-generating mechanisms are based on the jet's internal shock cell structure, and also in high-speed aerodynamics, since the interaction between internal jet flow and external pressure field can cause considerable aerodynamic interference with aircraft components. However, the present situation is quite similar to the case of duct flow: a complete formal solution only exists for a single special case, and because of mathematical difficulties, this particular solution has not even been completely evaluated yet.

Based on the fundamental works of Prandtl (1904) and Lord Rayleigh (1916), D.C. Pack (1950) was the first to calculate a formal solution for the case of an axisymmetric free jet emerging with constant over- or underpressure from a circular nozzle into a medium at rest. By superposition of the elementary modes resulting from a separation ansatz for the linearized equations of motion, he obtained the solution in the form of an infinite Fourier–Bessel series. Ward (1955) investigated the general properties of Pack's solution and found that there are periodically distributed discontinuities and singularities in the flow field, quite analoguous to those found for duct flow, which also make numerical evaluation a formidable problem by causing non-uniform convergence of the associated infinite series. Consequently, Pack's solution remained practically almost useless for several decades. The situation was partially improved

when Grabitz (1975) succeeded in evaluating at least the series associated with the density field by applying an analytical comparison method to improve the convergence of the corresponding infinite series. In a subsequent paper, Grabitz, Hiller & Meier (1979) compared theoretical Mach–Zehnder interferograms obtained by numerical integration of the theoretical density field with experimental images. Although the spatial resolution of the theoretical interferograms is rather low and the experimental images are strongly disturbed by turbulent mixing in the free shear layer, their results indicate that linear potential theory may well be adequate to describe the real flow field at least in the portions close to the jet orifice. Nevertheless, there is still considerable uncertainty about its validity throughout the field.

Therefore, although the situation appears somewhat better than for duct flow, the linearized theory of supersonic free jet flow also lacks completeness. The general theory allowing the specification of arbitrary efflux conditions at the nozzle orifice is still missing. The only existing formal solution of Pack has not been evaluated completely yet, since the method of Grabitz applies only to the density field of this special case. Consequently, as has been recently mentioned by Powell (1992), although Pack's solution is known for several decades, its physical nature still lacks proper interpretation. In addition, further experimental evidence about the validity of linear theory is highly desirable.

By extending the methods developed for duct flow in Part 1, the present paper intends to fill this gap. In § 2, the physical problem is formulated as an initial boundary value problem for the wave equation and its general solution, which has not been available so far, is derived. The singular behaviour of the solution and its physical meaning are investigated in § 3. By extending Kummer's series transformation to the present problem (and thus generalizing Grabitz's comparison method), the problems associated with non-uniformly converging series, which have prevented the unrestricted practical application of linear theory in the past, are completely resolved. For a physical interpretation of the resulting flow fields, the asymptotic reflection and transmission behaviour of small perturbations is investigated in § 4. Pack's classical solution and its most simple three-dimensional counterpart are evaluated and extensively discussed in § 5. For Pack's axisymmetric solution, theoretical Mach–Zehnder interferograms are calculated in § 6 by *analytical* integration of the density field and are compared with time-averaged images obtained from experiment. Finally, the formula for the wavelength of a supersonic free jet is derived and compared with experiment, and it is shown that the well-known formula of Pack (1950) is wrong, since it is based on an invalid interpretation of the jet's spatial structure.

2 General theory

2.1. *Mathematical formulation*

In the following, we consider a supersonic jet of gas issuing from a nozzle into a resting medium of ambient pressure p_0. The pressure difference between the inner portions of the jet and the surrounding medium is assumed to be small; thus, any shocks occurring in the flow can be assumed to be weak. The nozzle exit cross-section is assumed to be circular with radius R_0 (or to deviate only slightly therefrom). In consequence of these basic assumptions, the jet contour will be very close to a circular cylinder of radius R_0 and thus the flow can be interpreted as a superposition of an ideally expanded uniform parallel flow separated from the ambient medium by a

cylindrical vortex sheet and small pertubations, which can be assumed to be isentropic and irrotational if viscosity and heat conduction are neglected. Consequently, the flow is governed by the basic equations of linear potential theory in the same form as for duct flow.

In order to avoid referring to equations of Part 1, these relations are briefly repeated in the following. Let w_0 be the velocity of the ideally expanded parallel flow with Mach number $M_0 > 1$. Take a system of dimensionless cylindrical polar coordinates (r, φ, ζ) normalized with R_0 and $R_0(M_0^2 - 1)^{1/2}$ in the radial and axial directions respectively, such that the ζ-axis coincides with the jet axis and $\zeta = 0$ at the exit cross-section of the nozzle. Because of the fundamental assumption of irrotationality, there exists a scalar potential $\phi(r, \varphi, \zeta)$ of the perturbation velocity vector, which obeys the wave equation:

$$\frac{\partial^2 \phi}{\partial r^2} + \frac{1}{r}\frac{\partial \phi}{\partial r} + \frac{1}{r^2}\frac{\partial^2 \phi}{\partial \varphi^2} - \frac{\partial^2 \phi}{\partial \zeta^2} = 0 \tag{2.1}$$

and which is connected with the velocity components u, v, w in the (r, φ, ζ)-system via

$$\frac{u}{w_0} = \frac{\partial \phi}{\partial r}, \quad \frac{v}{w_0} = \frac{1}{r}\frac{\partial \phi}{\partial \varphi}, \quad \frac{w}{w_0} = 1 + \frac{1}{(M_0^2 - 1)^{1/2}}\frac{\partial \phi}{\partial \zeta}. \tag{2.2a–c}$$

Note that so far no assumption has been made about the thermodynamic equation of state of the flow medium. By assuming an ideal gas with constant ratio κ of the specific heats, the thermodynamic variables of state – pressure p, density ρ and temperature T – depend in linear approximation only on the *axial* velocity perturbation:

$$\frac{p}{p_0} = 1 - \frac{\kappa M_0^2}{(M_0^2 - 1)^{1/2}}\frac{\partial \phi}{\partial \zeta}, \tag{2.3a}$$

$$\frac{\rho}{\rho_0} = 1 - \frac{M_0^2}{(M_0^2 - 1)^{1/2}}\frac{\partial \phi}{\partial \zeta}, \tag{2.3b}$$

$$\frac{T}{T_0} = 1 - \frac{(\kappa - 1) M_0^2}{(M_0^2 - 1)^{1/2}}\frac{\partial \phi}{\partial \zeta}, \tag{2.3c}$$

with p_0, ρ_0 and T_0 denoting the pressure, density and temperature in the ideally expanded parallel flow, respectively.

So far, the governing equations are formally identical with those describing the supersonic flow in the interior of a cylindrical duct. The fundamental physical difference between the two types of flow manifests itself in different boundary conditions. In the case of a duct, the velocity vector at the wall must be tangential to the prescribed contour, whereas for a free jet the existence conditions of an ideal vortex sheet separating a flow from a medium at rest require the pressure at the jet boundary to be continuous (cf. Ward 1955). Consequently, from (2.3*a*), this condition can be formulated as

$$\left.\frac{\partial \phi}{\partial \zeta}\right|_{r=1} = 0, \qquad \zeta > 0. \tag{2.4}$$

However, equation (2.4) is not the proper mathematical form of the boundary condition, since it does not guarantee the continuity of the velocity potential at the nozzle edge $r = 1$, $\zeta = 0$, which must be fulfilled at *any* location in the field, even in the case of discontinuities (shocks) being present in the flow (Ward 1955). Therefore, the appropriate form of the boundary condition implying (2.4) is

$$\phi|_{r=1} = \phi(1, \varphi, 0), \qquad \zeta > 0. \tag{2.5}$$

In order to complete the initial-boundary value problem for the wave equation (2.1), we further have to specify the functional form of both the velocity potential ϕ and its first derivative with respect to ζ at $\zeta = 0$. Physically, this means that the components (2.2) of the velocity perturbation vector must be known in the nozzle exit cross-section. Hence, the mathematical description of supersonic free jet flow is formally reduced to a Cauchy problem for the wave equation similar to that obtained for duct flow in Part 1, the only difference consisting in the boundary condition (2.5) prescribing the velocity potential at $r = 1$ instead of its normal derivative.

2.2. *General solution*

The general solution of the inhomogeneous initial-boundary value problem specified in the preceeding subsection can be found in a quite similar way as in Part 1, viz. by using the eigenfunctions and eigenvalues of the associated homogeneous problem. From a separation ansatz for the wave equation (2.1) involving the homogeneous form of the boundary condition (2.5)

$$\phi|_{r=1} = 0, \tag{2.6}$$

the velocity potential $\phi(r, \varphi, \zeta)$ is obtained in the following form:

$$\phi(r, \varphi, \zeta) = \sum_{m=0}^{\infty} \sum_{n=1}^{\infty} J_m(\beta_{mn} r)\, [A_{mn}(\zeta) \cos m\varphi + B_{mn}(\zeta) \sin m\varphi], \tag{2.7}$$

where $J_m(x)$ are the Bessel functions of first kind and integer order m and the β_{mn} denote the real positive zeros of $J_m(x)$ arranged in ascending order of magnitude. By utilizing the orthogonality properties of the Bessel and the harmonic functions, the following complex relation between the coefficient functions $A_{mn}(\zeta)$, $B_{mn}(\zeta)$ is easily derived from (2.7):

$$\begin{aligned} C_{mn}(\zeta) &:= A_{mn}(\zeta) + \mathrm{i}\, B_{mn}(\zeta) \\ &= \frac{2}{\pi J_{m+1}^2(\beta_{mn})} \int_0^{2\pi} \int_0^1 r\, \phi(r, \varphi, \zeta)\, J_m(\beta_{mn} r)\, \mathrm{e}^{\mathrm{i} m\varphi}\, \mathrm{d}r\mathrm{d}\varphi, \end{aligned} \tag{2.8}$$

where for $m = 0$, the right-hand side has to be divided by 2. Now, by integrating (2.8) twice by parts with respect to r and ζ respectively, we obtain

$$\begin{aligned} C_{mn}(\zeta) = \frac{2}{\pi J_{m+1}^2(\beta_{mn})} \Bigg\{ & \frac{J_{m+1}(\beta_{mn})}{\beta_{mn}} \int_0^{2\pi} \phi|_{r=1}\, \mathrm{e}^{\mathrm{i} m\varphi}\, \mathrm{d}\varphi \\ & - \frac{1}{\beta_{mn}^2} \int_0^{2\pi} \int_0^1 r \left[\frac{\partial^2 \phi}{\partial r^2} + \frac{1}{r} \frac{\partial \phi}{\partial r} + \frac{1}{r^2} \frac{\partial^2 \phi}{\partial \varphi^2} \right] J_m(\beta_{mn} r)\, \mathrm{e}^{\mathrm{i} m\varphi}\, \mathrm{d}r\mathrm{d}\varphi \Bigg\}, \end{aligned} \tag{2.9}$$

while on the other hand, differentiating (2.8) twice with respect to ζ yields ($C''_{mn}(\zeta)$ denotes $\mathrm{d}^2 C_{mn}/\mathrm{d}\zeta^2$)

$$C''_{mn}(\zeta) = \frac{2}{\pi J_{m+1}^2(\beta_{mn})} \int_0^{2\pi} \int_0^1 r \frac{\partial^2 \phi}{\partial \zeta^2} J_m(\beta_{mn} r)\, \mathrm{e}^{\mathrm{i} m\varphi}\, \mathrm{d}r\mathrm{d}\varphi, \tag{2.10}$$

so that after multiplying (2.9) with β_{mn}^2, adding the result to (2.10) and using both the

wave equation (2.1) and the boundary condition (2.5), we finally obtain the simple result

$$C''_{mn} + \beta^2_{mn} C_{mn} = \frac{2\beta_{mn}}{\pi J_{m+1}(\beta_{mn})} \int_0^{2\pi} \phi(1, \varphi, 0)\ \mathrm{e}^{\mathrm{i}m\varphi}\, \mathrm{d}\varphi. \tag{2.11}$$

Note that as above, the right-hand side has to be divided by 2 for $m = 0$. Thus, as in the case of duct flow, the coefficient functions $A_{mn}(\zeta)$, $B_{mn}(\zeta)$ of the velocity potential (2.7) are given as solutions of the inhomogeneous differential equation (2.11) for a mass–spring system. Since the right-hand side of (2.11) does not depend on ζ, it is straightforward to establish the general solution (2.7) in terms of the physical initial conditions, but the resulting expressions are rather lengthy and are therefore not reported here.

2.3. *Solutions with harmonic azimuthal dependence*

In order to simplify the further considerations, we will as in Part 1 restrict the discussion to problems where the functional dependence of the velocity potential on the azimuthal angle φ is given by the single harmonic function $\cos m\varphi$ ($m = 0, 1, 2 \ldots$). For these cases, the general velocity potential (2.7) simplifies to

$$\phi(r, \varphi, \zeta) = \cos m\varphi \sum_{n=1}^{\infty} A_{mn}(\zeta)\, J_m(\beta_{mn} r) = \phi_m(r, \zeta) \cos m\varphi. \tag{2.12}$$

By solving the ordinary differential equation (2.11) for this special case, incorporating the initial conditions at the nozzle exit $\zeta = 0$

$$\phi(r, \varphi, 0) = \phi_m(r, 0) \cos m\varphi, \tag{2.13a}$$

$$\left.\frac{\partial \phi}{\partial \zeta}\right|_{\zeta=0} = \phi'_m(r, 0) \cos m\varphi \tag{2.13b}$$

via the integral relation (2.8) and using the known series (cf. Watson 1944)

$$\sum_{n=1}^{\infty} \frac{2 J_m(\beta_{mn} r)}{\beta_{mn} J_{m+1}(\beta_{mn})} = r^m, \tag{2.14}$$

the main part $\phi_m(r, \zeta)$ of (2.12) can be written as

$$\phi_m(r, \zeta) = \phi_m(1, 0)\, r^m + \sum_{n=1}^{\infty} J_m(\beta_{mn} r)\, [a^1_{mn} \cos \beta_{mn}\zeta + a^2_{mn} \sin \beta_{mn}\zeta] \tag{2.15}$$

with the coefficients a^1_{mn}, a^2_{mn} being given by

$$a^1_{mn} = \frac{2}{J^2_{m+1}(\beta_{mn})} \int_0^1 r\, [\phi_m(r, 0) - r^m \phi_m(1, 0)]\, J_m(\beta_{mn} r)\, \mathrm{d}r, \tag{2.16a}$$

$$a^2_{mn} = \frac{2}{\beta_{mn} J^2_{m+1}(\beta_{mn})} \int_0^1 r\, \phi'_m(r, 0)\, J_m(\beta_{mn} r)\, \mathrm{d}r. \tag{2.16b}$$

Thus, via (2.15) and (2.16), the velocity potential (2.12) has been related to the physical initial conditions (2.13), i.e. to the velocity perturbation vector at the nozzle exit $\zeta = 0$. Once their functional form has been known either from experiment or by theoretical argumentation, the integrals in (2.16) can be evaluated and the complete flow field can be determined by (2.2) and (2.3), which relate the velocity potential to the physical flow variables.

3 The singularities of cylindrical supersonic free jet flow

3.1. *Conditions for the occurrence of singularities*

Like the case of duct flow, the linearized theory of free jet flow can under certain circumstances provide singular solutions, the singularities being representative of phenomena the theory is unable to describe correctly, viz. shock and expansion waves of finite amplitude. This has qualitatively been pointed out by Ward (1955) and later has been confirmed by Grabitz (1975) for the special case of the density field provided by Pack's solution. Although the existence of singularities in the flow might appear as a point of merely academic interest at a first glance, it is associated with a very serious practical problem. The occurrence of singularities in functions described by infinite series gives rise to non-uniform convergence and thus to oscillatory behaviour of the partial sums ('Gibbs' phenomenon') of these series, thus making their precise numerical evaluation by direct summation impracticable in spite of the great computational power available today. In Part 1, it has been shown for the series associated with duct flow that this problem can completely be resolved by isolating the singular parts of any given solution in a universal series, which itself is evaluated by Kummer's series transformation. Therefore, the aim of the following considerations is to extend this method to the present problem.

As in Part 1, we will restrict the further discussion to velocity potentials of the form (2.12), where the azimuthal dependence is given by a single harmonic function, whereas the radial and axial dependence is described by an infinite series of the form

$$\phi_m(r,\zeta) = \sum_{n=1}^{\infty} A_{mn} J_m(\beta_{mn} r) \tag{3.1}$$

with the coefficients A_{mn} being functions of the axial coordinate ζ. Series of the form (3.1) are known as Fourier–Bessel series (of the first kind) and are well established in the mathematical literature (Watson 1944; Tolstov 1976). Their convergence behaviour is conveniently investigated by the basic relation (Tolstov 1976)

$$|A_{mn}| \leqslant \frac{L}{\beta_{mn}^{p+\varepsilon}} \tag{3.2}$$

which, for sufficiently large n, must be fulfilled with L being some positive constant and $0 < \varepsilon < 1$ in order to guarantee uniform convergence of (3.1) and its first $p-1$ derivatives with respect to r in $[0,1]$. Thus, in order to apply (3.2) to velocity potentials of the form (2.12), the large-n asymptotic form of the coefficient integrals (2.16) has to be determined. By using analytical standard methods, which are described in detail elsewhere (chapter 6 of Bleistein & Handelsman 1986), we obtain the following asymptotic expansion valid for integrals of the type (2.16):

$$\int_0^1 r\,\chi(r)\,J_m(\beta_{mn} r)\,\mathrm{d}r = \frac{\chi(1)}{\beta_{mn}} J_{m+1}(\beta_{mn}) + O\left(\frac{1}{\beta_{mn}^{7/2}}\right) \tag{3.3}$$

provided that $\chi(r)$ is continuous in $[0,1]$ and $\chi(0) = 0$ except for $m = 0$, where finite values are allowed. Now, by substituting (3.3) into (2.16) and considering the inequality (Tolstov 1976)

$$|J_{m+1}(\beta_{mn})| \geqslant \frac{L}{(\beta_{mn})^{1/2}} \tag{3.4}$$

with L denoting some positive constant, we finally get the large-n asymptotic form of the coefficient integrals (2.16):

$$a^1_{mn} = O\left(\frac{1}{\beta^{5/2}_{mn}}\right), \tag{3.5a}$$

$$a^2_{mn} = \frac{2\,\phi'_m(1,0)}{\beta^2_{mn}\,J_{m+1}(\beta_{mn})} + O\left(\frac{1}{\beta^{7/2}_{mn}}\right). \tag{3.5b}$$

From (3.4), it is clear that the first term on the right-hand side of (3.5*b*) varies as $\beta^{-3/2}_{mn}$, and since

$$\left|\sin\beta_{mn}\zeta\right| \leqslant 1, \tag{3.6}$$

we can using (3.2) draw the important conclusion that non-uniform convergence of the first derivatives of (2.15) occurs whenever $\phi'_m(1,0) \neq 0$, i.e. when a discontinuity of $\partial\phi/\partial\zeta$ occurs at the nozzle edge $r = 1$, $\zeta = 0$. Physically, this means because of (2.3*a*) that ideal expansion *at the nozzle edge* (i.e. not necessarily in the inner portions of the nozzle exit cross-section) is sufficient to guarantee a bounded continuous solution throughout the field.

Therefore, in a similar manner as in Part 1, by defining the universal series

$$S_m(r,\zeta) = \sum_{n=1}^{\infty} \frac{2\,J_m(\beta_{mn}r)\,\sin\beta_{mn}\zeta}{\beta^2_{mn}\,J_{m+1}(\beta_{mn})}, \tag{3.7}$$

we can decompose *any* function (2.15) by suitable addition and subtraction of (3.7) in the following manner:

$$\phi_m(r,\zeta) = \phi'_m(1,0)\,S_m(r,\zeta) + \phi_m(1,0)\,r^m + \sum_{n=1}^{\infty} a^1_{mn}\,J_m(\beta_{mn}r)\cos\beta_{mn}\zeta$$
$$+ \sum_{n=1}^{\infty}\left[a^2_{mn} - \frac{2\,\phi'_m(1,0)}{\beta^2_{mn}\,J_{m+1}(\beta_{mn})}\right] J_m(\beta_{mn}r)\,\sin\beta_{mn}\zeta \tag{3.8}$$

with the first term on the right-hand side containing all singularities and discontinuities caused by non-uniform convergence, while all the remaining terms correspond to bounded continuous functions with bounded continuous first derivatives. Hence, both the discussion of singular behaviour and the problem of evaluating non-uniformly converging series have been shifted to the series $S_m(r,\zeta)$, whose universal character has thus become obvious.

3.2. *The evaluation of the first derivatives of* $S_m(r,\zeta)$ *and their singular behaviour*

In Part 1, the problem of evaluating the non-uniformly converging series associated with supersonic duct flow has successfully been resolved by the extension of a well-established analytical tool, viz. Kummer's series transformation, to Dini series. Therefore, it appears appropriate to apply this method also to the Fourier–Bessel series connected with supersonic free jet flow. The basic idea behind Kummer's series

transformation is as follows: having given a non-uniformly converging series S for evaluation

$$S = \sum_{n=1}^{\infty} s_n \tag{3.9}$$

one has to find a suitable so-called comparison series

$$\widetilde{S} = \sum_{n=1}^{\infty} \tilde{s}_n \tag{3.10}$$

whose terms are asymptotically related to the terms of (3.9) in the following manner:

$$s_n = \tilde{s}_n + O\left(\frac{1}{n^{1+\varepsilon}}\right), \qquad \varepsilon > 0, \tag{3.11}$$

and which thus exhibits about the same poor convergence, but whose sum $\widetilde{S}$ is *known in closed analytical form.* Then, by subtracting (3.10) from (3.9), we get

$$S = \widetilde{S} + \sum_{n=1}^{\infty} (s_n - \tilde{s}_n) \tag{3.12}$$

and are thus left with the numerical evaluation of a series which by (3.11) converges *uniformly*, while all the singularities (and therefore, all problems arising from non-uniform convergence) are now buried in the *closed* expression $\widetilde{S}$. Hence, by adopting the notation introduced in (3.9)–(3.12) and writing the first derivatives of $S_m(r,\zeta)$ in the form

$$S_{m,r}(r,\zeta) := \frac{\partial S_m(r,\zeta)}{\partial r} = \sum_{n=1}^{\infty} s_{mn,r}(r,\zeta), \tag{3.13a}$$

$$S_{m,\zeta}(r,\zeta) := \frac{\partial S_m(r,\zeta)}{\partial \zeta} = \sum_{n=1}^{\infty} s_{mn,\zeta}(r,\zeta) \tag{3.13b}$$

with $s_{mn,r}(r,\zeta)$, $s_{mn,\zeta}(r,\zeta)$ denoting the derivatives of the terms of (3.7), we have to find appropriate comparison terms $\tilde{s}_{mn,r}(r,\zeta)$, $\tilde{s}_{mn,\zeta}(r,\zeta)$ which have the desired asymptotic behaviour (3.11) and, furthermore, can be summed to closed expressions $\widetilde{S}_{m,r}(r,\zeta)$, $\widetilde{S}_{m,\zeta}(r,\zeta)$, so that Kummer's series transformation (3.12) can be applied in a straightforward manner.

By adopting the same procedure as in Part 1, this task can be solved by replacing the Bessel functions, their derivatives and their zeros by their well-known asymptotic expansions (cf. Abramowitz & Stegun 1972) :

$$J_m(x) \sim +\left(\frac{2}{\pi x}\right)^{1/2} \cos(x - m\pi/2 - \pi/4) + O\left(\frac{1}{x^{3/2}}\right), \tag{3.14a}$$

$$J'_m(x) \sim -\left(\frac{2}{\pi x}\right)^{1/2} \sin(x - m\pi/2 - \pi/4) + O\left(\frac{1}{x^{3/2}}\right), \tag{3.14b}$$

$$\beta_{mn} \sim \mu_{mn} + O\left(\frac{1}{\mu_{mn}}\right), \qquad \mu_{mn} := (n + m/2 - 1/4)\pi, \tag{3.14c}$$

thus expressing $s_{mn,r}(r,\zeta)$, $s_{mn,\zeta}(r,\zeta)$ in terms of harmonic functions, which can be summed to closed expressions by using the classical analytical methods available for

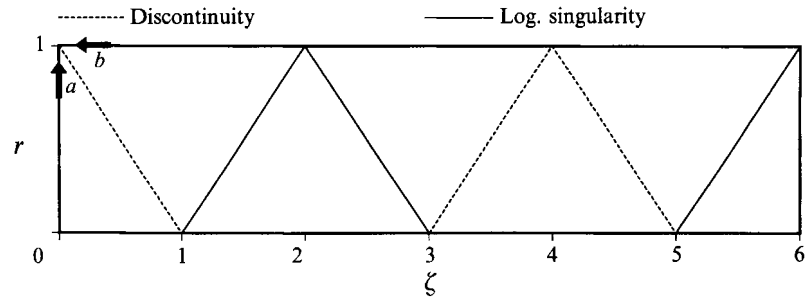

FIGURE 1. Location of singularities in the (r,ζ)-plane. Arrows *a* and *b* indicate the limiting process used in obtaining equations (3.15) and (3.16), respectively.

Fourier series. Since however the corresponding expressions are somewhat lengthy and provide nothing new from the physical point of view, they are not given here but reported in the Appendix. With the closed comparison sums (A 6), the singular behaviour of the series $S_{m,r}(r,\zeta)$, $S_{m,\zeta}(r,\zeta)$ can conveniently be discussed, while by using the comparison terms (A 5), their numerical evaluation via Kummer's series transformation (3.12) represents no serious problem any more.

From equation (A 6) it is therefore easily established that for $r > 0$, $S_{m,r}(r,\zeta)$ and $S_{m,\zeta}(r,\zeta)$ exhibit exactly the same singularity pattern as found in Part 1 for duct flow, viz. discontinuities at $(r\pm\zeta-1) = 4k$ and logarithmic poles at $(r\pm\zeta-1) = 4k+2$, with k being an integer number. The corresponding pattern is illustrated in figure 1. Also, $S_{0,\zeta}$ and $S_{1,r}$ exhibit inverse-square-root singularities on the axis $r = 0$ at $\zeta = 1, 3, 5...$, respectively. Following (3.8), these singularities are present in the flow whenever there is a discontinuity of pressure at the nozzle edge and therefore, in physical reality, shock and expansion wave patterns are produced, whose spatial structure closely resembles the singularity pattern illustrated in figure 1. Thus, as in the case of duct flow, linear potential theory itself seems to indicate the locations where it fails to describe physical phenomena adequately.

Finally, the question of the discontinuous changes of the velocity components at the nozzle edge $r = 1$, $\zeta = 0$ is of special interest since one expects intuitively that at this location, the conditions of the Prandtl–Meyer expansion are fulfilled. From (A 6) it is easily derived that on approaching $r = 1$ from the left-hand side of the r-axis at $\zeta = 0$ (cf. figure 1, arrow *a*), we have

$$\left.\begin{aligned} \tilde{S}_{m,r}(1-0,0) &= -[\Psi_m(-0) - \Psi_m(-0)] = 0, \\ \tilde{S}_{m,\zeta}(1-0,0) &= -[\Psi_m(-0) + \Psi_m(-0)] = 1, \end{aligned}\right\} \tag{3.15}$$

whereas on approaching $\zeta = 0$ from the right-hand side of the ζ-axis at $r = 1$, we get (cf. figure 1, arrow *b*)

$$\left.\begin{aligned} \tilde{S}_{m,r}(1,+0) &= -[\Psi_m(+0) - \Psi_m(-0)] = -1, \\ \tilde{S}_{m,\zeta}(1,+0) &= -[\Psi_m(+0) + \Psi_m(-0)] = 0, \end{aligned}\right\} \tag{3.16}$$

since according to (A 7), the function $\Psi_m(x)$ varies as $\frac{1}{2}\operatorname{sgn} x$ in the vicinity of $x = 0$. From (2.12), (3.8) and (2.2), it is thus easily established that the azimuthal velocity v

is continuous at the nozzle edge, while the ratio of the discontinuous changes of the radial and axial velocities u and w is in any half-plane $\varphi = const.$ given by

$$\frac{u(1,\varphi,+0)-u(1-0,\varphi,0)}{w(1,\varphi,+0)-w(1-0,\varphi,0)} = (M_0^2-1)^{1/2}. \tag{3.17}$$

This is the well-known Ackeret relation, which indeed represents the Prandtl–Meyer condition for the case of small perturbations of a uniform parallel flow with Mach number M_0 (Oswatitsch 1952).

4 Asymptotic reflection and transmission laws

By means of the methods described in the previous sections, we are now able to derive and evaluate supersonic free jet flow fields of interest. However, in order to also be able to interpret the physical nature of the results, we will first study the general rules which govern the propagation of small perturbations along the characteristics of the wave equation. When substituting the general form (2.12) of the velocity potential for solutions with harmonic azimuthal dependence into (2.1), we obtain a hyperbolic partial differential equation for the function $\phi_m(r,\zeta)$ with characteristics given by

$$r \pm \zeta = const. \tag{4.1}$$

which, in three dimensions, represents an infinite set of characteristic surfaces, each of them consisting of Mach cones being arranged coaxial to the jet axis $r = 0$, with their base circles and vertices coinciding in an alternating manner (cf. figure 5 of Part 1). From (2.11), it is clear that the coefficients $A_{mn}(\zeta)$ will essentially be given by harmonic functions, so that a single elementary mode $\phi_{mn}(r,\varphi,\zeta)$ of the velocity potential (2.12) can in complex form be written as

$$\phi_{mn}(r,\varphi,\zeta) = J_m(\beta_{mn}r)\,e^{i\beta_{mn}\zeta}\cos m\varphi\,. \tag{4.2}$$

By substituting the asymptotic expansions (3.14) for the Bessel function $J_m(x)$ and their zeros β_{mn} into (4.2), $\phi_{mn}(r,\varphi,\zeta)$ can be asymptotically decomposed into two parts propagating on the characteristics $r+\zeta = const.$ and $r-\zeta = const.$, respectively:

$$\phi_{mn}(r,\varphi,\zeta) \sim \Phi^+(r,\varphi,\zeta) + \Phi^-(r,\varphi,\zeta), \tag{4.3}$$

where

$$\Phi^{\pm}(r,\varphi,\zeta) = \pm(-1)^{n+1}\left(\frac{2}{\pi\mu_{mn}r}\right)^{1/2}\frac{i}{2}\,e^{\pm i\mu_{mn}(r\pm\zeta-1)}\cos m\varphi\,,$$

which closely resembles the corresponding relation (4.4) derived in §4 of Part 1. By means of (4.3), the asymptotic reflection and transmission behaviour of small physical perturbations can be investigated in the same manner as in the case of duct flow by considering only the downstream component on a particular characteristic.

Consider a small harmonic perturbation which originates at the jet boundary $r = 1$ at an arbitrary location $\zeta = \zeta^* - 1$, $\varphi = \varphi_0$ and is travelling towards the axis on the characteristic $r+\zeta = \zeta^*$. If we substitute this path of propagation into the corresponding part of (4.3), we obtain (C denotes a constant)

$$\Phi^+(r,\varphi,\zeta) = \frac{C}{r^{1/2}}\,e^{i\mu_{mn}(\zeta^*-1)}\cos m\varphi_0\,. \tag{4.4}$$

At $r = 0$, the perturbation crosses the axis and enters the half-plane $\varphi = \varphi_0 + \pi$, thus

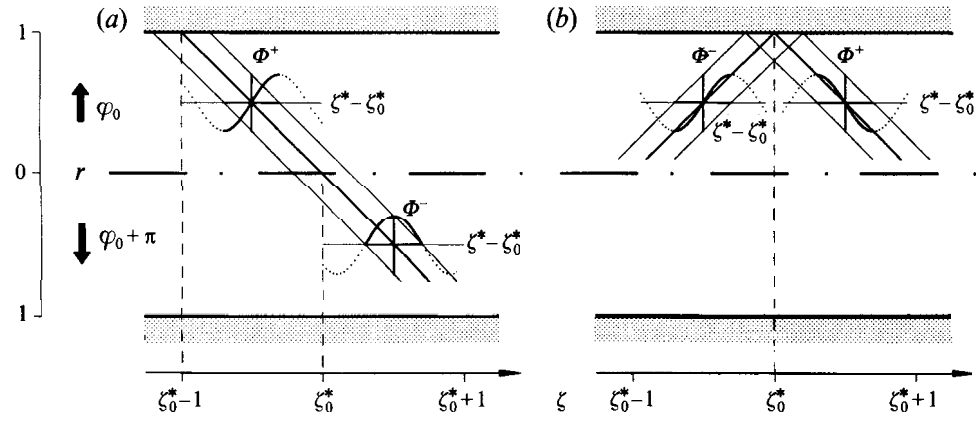

FIGURE 2. Asymptotic propagation laws for a sinusoidal perturbation. (*a*) Transmission through the axis $r = 0$ resulting in a phase shift of $\pi/2$; (*b*) reflection at the jet boundary $r = 1$ with a phase shift of π.

changing to the characteristic $r - \zeta = -\zeta^*$. Consequently, we obtain on considering (3.14*c*):

$$\Phi^-(r,\varphi,\zeta) = -\frac{C}{r^{1/2}}\,\mathrm{e}^{\mathrm{i}\mu_{mn}(\zeta^*+1)}\cos m(\varphi_0+\pi)$$
$$= \frac{C}{r^{1/2}}\,\mathrm{e}^{\mathrm{i}\mu_{mn}(\zeta^*-1)}\,\mathrm{e}^{\mathrm{i}\pi/2}\cos m\varphi_0\,, \tag{4.5}$$

and thus the result that upon crossing the axis, a perturbation suffers an asymptotical phase shift of $\pi/2$ as illustrated in figure 2(*a*) for an initially sinusoidal perturbation. This is not surprising since in Part 1 we had obtained the same result for the case of duct flow, which differs from the present problem only by the boundary condition.

Now we investigate the case where different results are to be expected, viz. the reflection of a perturbation at the jet boundary $r = 1$. On travelling from the axis to the boundary, the disturbance is propagating along the downstream characteristic $r - \zeta = 1 - \zeta^*$ in the half-plane φ_0. Hence, we obtain

$$\Phi^-(r,\varphi,\zeta) = -\frac{C}{r^{1/2}}\,\mathrm{e}^{\mathrm{i}\mu_{mn}\zeta^*}\cos m\varphi_0 \tag{4.6}$$

whereas after reflection, it remains in the same half-plane $\varphi = \varphi_0$ and changes to the characteristic $r + \zeta = 1 + \zeta^*$. This yields

$$\Phi^+(r,\varphi,\zeta) = \frac{C}{r^{1/2}}\,\mathrm{e}^{\mathrm{i}\mu_{mn}\zeta^*}\cos m\varphi_0$$
$$= -\frac{C}{r^{1/2}}\,\mathrm{e}^{\mathrm{i}\mu_{mn}\zeta^*}\,\mathrm{e}^{\mathrm{i}\pi}\cos m\varphi_0 \tag{4.7}$$

and thus an asymptotical phase shift of π, which means that at the jet boundary, the sign of a perturbation is just inverted. This reflection behaviour, which is illustrated in figure 2(*b*), is exactly opposite to that obtained for duct flow, where a perturbation is reflected unchanged at the wall.

Since, besides constant factors, the first derivatives of (4.2) with respect to ζ have the same functional form as (4.2) itself, the same results hold for all flow variables (2.2) and (2.3) except for radial velocity, which depends on $\partial\phi/\partial r$. A similar analysis on considering the asymptotic expansion (3.14*b*) for the derivative $J'_m(x)$ of the Bessel

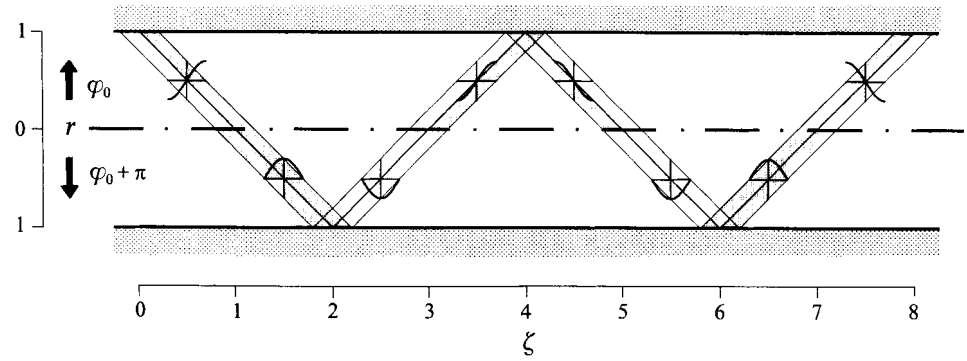

FIGURE 3. Asymptotic propagation laws for a sinusoidal density perturbation travelling through a cylindrical free jet. Areas of compression are indicated by shading.

function yields the result that a radial velocity perturbation suffers an asymptotical phase shift of $-\pi/2$ upon crossing the axis, while it is reflected unchanged (i.e. with zero phase shift) at the jet boundary.

Finally, in order to give a practical example comparable with figure 7 of Part 1, the propagation of an initially sinusoidal density perturbation is illustrated in figure 3. Starting at $r = 1$, $\varphi = \varphi_0$, $\zeta = 0$ as an expansion–compression wave (i.e. expansive on the upstream side and compressive on the downstream side of the leading characteristic), the perturbation is travelling towards the axis, where it is transformed into a purely compressive wave by a phase shift of $\pi/2$ when entering the half-plane $\varphi_0 + \pi$. Being reflected at the jet boundary $r = 1$, $\zeta = 2$, it suffers a phase shift of π, thus being transformed into a purely expansive wave which is travelling back towards the axis. When crossing the axis at $\zeta = 3$ and entering $\varphi_0 = \pi$, it again suffers a phase shift of $\pi/2$, which restores the initial sinusoidal shape. After inversion upon reflection at $r = 1$, $\zeta = 4$, the whole process is repeated with opposite sign, so that finally, after reflection at $r = 1$, $\zeta = 8$, the wave is again travelling towards the axis with sinusoidal shape and the whole cycle starts again.

Hence, besides the opposite reflection behaviour, we have obtained quite similar results as in the case of duct flow. For flow variables represented by a non-uniformly converging infinite series in terms of the elementary modes (4.2), the singular behaviour is determined solely by their large-n asymptotic form, so that a sinusoidal perturbation corresponds to a discontinuity, while a symmetric cosine variation will result in a logarithmic pole. Also, radial focusing effects are to be expected in the vicinity of a logarithmic singularity close to the axis, since the elementary modes vary asymptotically in magnitude as $r^{-1/2}$.

5 Elementary cases of supersonic free jet flow

By means of the theory derived in the previous sections, we are now able to calculate and discuss solutions for a great variety of axisymmetric and non-axisymmetric free jets. In this section, we will focus our attention on those kinds of jets whose velocity potential is solely determined by the series $S_m(r, \zeta)$ and which thus describe the most interesting features of supersonic free jet flow.

First, we have to find the particular initial conditions (2.13) which lead to the

desired velocity potential. It is easily verified from (2.12)–(2.16) that by specifying

$$\phi(r,\varphi,0)=0, \tag{5.1a}$$

$$\left.\frac{\partial\phi}{\partial\zeta}\right|_{\zeta=0}=-\frac{(M_0^2-1)^{1/2}}{\kappa M_0^2}\frac{\Delta p}{p_0}r^m\cos m\varphi, \tag{5.1b}$$

which corresponds to a free jet emerging from the nozzle in parallel flow with the pressure perturbation in the exit cross-section being given by $\Delta p\, r^m \cos m\varphi$ ($\Delta p = const.$), we obtain the velocity potential

$$\phi(r,\varphi,\zeta)=-\frac{(M_0^2-1)^{1/2}}{\kappa M_0^2}\frac{\Delta p}{p_0}\cos m\varphi\sum_{n=1}^{\infty}\frac{2J_m(\beta_{mn}r)\sin\beta_{mn}\zeta}{\beta_{mn}^2 J_{m+1}(\beta_{mn})}$$

$$=-\frac{(M_0^2-1)^{1/2}}{\kappa M_0^2}\frac{\Delta p}{p_0}S_m(r,\zeta)\cos m\varphi. \tag{5.2}$$

From (2.2) and (2.3), all physical flow variables of interest can now be computed in a straightforward manner. By introducing dimensionless perturbations $\delta\rho(r,\varphi,\zeta)$ and $\delta u(r,\varphi,\zeta)$ of density and radial velocity respectively, we obtain for example

$$\frac{\rho}{\rho_0}=1+\frac{1}{\kappa}\frac{\Delta p}{p_0}\delta\rho(r,\varphi,\zeta), \tag{5.3a}$$

$$\frac{u}{w_0}=\frac{(M_0^2-1)^{1/2}}{\kappa M_0^2}\frac{\Delta p}{p_0}\delta u(r,\varphi,\zeta), \tag{5.3b}$$

where

$$\delta\rho(r,\varphi,\zeta)=S_{m,\zeta}(r,\zeta)\cos m\varphi, \tag{5.4a}$$

$$\delta u(r,\varphi,\zeta)=-S_{m,r}(r,\zeta)\cos m\varphi. \tag{5.4b}$$

Furthermore, it is of interest to know what shapes of the jet boundary are predicted by linear potential theory. By reversing the argumentation used in Part 1 to derive the boundary condition (2.6) for supersonic flow in ducts, we obtain the general result that the envelope surface of all streamlines originating at $r = r_0$ in the nozzle exit cross-section $\zeta = 0$ is to a first order of approximation given by

$$r(r_0,\varphi,\zeta)=r_0+\lambda(r_0,\varphi,\zeta) \tag{5.5a}$$

where

$$\lambda(r_0,\varphi,\zeta)=(M_0^2-1)^{1/2}\int_0^{\zeta}\left.\frac{\partial\phi}{\partial r}\right|_{r=r_0}\mathrm{d}\zeta, \qquad 0<r_0\leqslant 1. \tag{5.5b}$$

Thus, the shape of a particular streamtube can be determined by simply integrating the radial velocity perturbation, which gives the approximate streamline slope.

Hence, by performing the integration (5.5*b*) with (5.3*b*) at $r_0 = 1$, we obtain the shape of the jet boundary:

$$\lambda(1,\varphi,\zeta)=\frac{\Delta p}{p_0}\frac{M_0^2-1}{\kappa M_0^2}\delta r(1,\zeta)\cos m\varphi \tag{5.6}$$

where

$$\delta r(1,\zeta)=\sum_{n=1}^{\infty}\frac{2(1-\cos\beta_{mn}\zeta)}{\beta_{mn}^2}. \tag{5.7}$$

Since (5.5*b*) is not defined for $r_0 = 0$, we have to consider this case separately. By transforming the velocity vector into Cartesian coordinates and using the limit relations of the Bessel functions $J_m(x)$ for $x \to 0$ (cf. Abramowitz & Stegun 1972), it is straightforward to verify that the radial and azimuthal velocity on the axis both vanish for all m except $m = 1$ and that in this case, the velocity vector at $r_0 = 0$ remains in the plane $\varphi = 0, \pi$. Consequently, the axis streamline also remains in this plane and we obtain

$$\lambda(0,\zeta) = \frac{\Delta p}{p_0} \frac{M_0^2 - 1}{\kappa M_0^2} \delta r(0,\zeta) \tag{5.8}$$

with

$$\delta r(0,\zeta) = \begin{cases} \displaystyle\sum_{n=1}^{\infty} \frac{\cos \beta_{1n}\zeta - 1}{\beta_{1n}^2 J_2(\beta_{1n})}, & m = 1 \\ 0, & \text{otherwise} \end{cases} \tag{5.9}$$

for the distortion of the axial streamline in $\varphi = 0, \pi$.

In the case $m = 0$, the velocity potential (5.2) describes an axisymmetric free jet emerging with constant under- or overpressure Δp in the nozzle cross-section. Although the first formal solution of this problem by Pack (1950) has been known for several decades, it has not been evaluated completely until now because of the problems associated with the non-uniform convergence of the first derivatives of $S_m(r,\zeta)$ (cf. § 3). By means of Kummer's series transformation, these difficulties are now completely resolved and all physical flow variables of interest can be readily determined and discussed.

The corresponding numerical results are graphically illustrated in figure 4. The geometry of the problem is shown in figure 4(*a*) for an underexpanded (i.e. $\Delta p > 0$) free jet, where (5.7) has been used to give an approximate idea of its boundary shape. Figure 4(*b*) presents the dimensionless perturbation (5.4*a*) of density, while figure 4(*c*) shows the dimensionless perturbation (5.4*b*) of radial velocity and also the dimensionless distortion (5.7) of the boundary streamlines, which essentially represents the integral of (5.4*b*) with respect to ζ. It is therefore clear that the logarithmic poles of radial velocity correspond to inflection points of $\delta r(1,\zeta)$, while the discontinuities of $\delta u(1,\zeta)$ give rise to kinks in the jet contour. Finally, in order to provide an impression of the radial density profiles, figure 5 additionally presents surface plots of $\delta\rho(r,\zeta)$ in the semicircle $0 \leqslant r \leqslant 1$, $0 \leqslant \varphi \leqslant \pi$ for various locations $\zeta = const.$

The obtained results are quite similar to those for duct flow (cf. Part 1) and can in an analoguous manner be qualitatively explained by the asymptotic propagation laws derived in § 4. When leaving the nozzle with slight overpressure, the boundary streamlines are bent outwards abruptly, and consequently a discontinuous expansion wave is propagating along the downstream surface of the leading Mach cone with base circle in $\zeta = 0$ and vertex in $\zeta = 1$, while the flow inside the cone remains undisturbed. By radial focusing, the magnitude of the expansion wave increases strongly as the axis is approached. When crossing the axis at $\zeta = 1$, the discontinuous compression–expansion wavefront is transformed into a symmetric, purely expansive wave to generate a region of extremely low density in the downstream vicinity of $r = 0$, $\zeta = 1$. At the jet boundary $r = 1$, $\zeta = 2$, the purely expansive wave is inverted into a purely compressive wave, which ends up in a region of extremely high density at the axis in the upstream vicinity of $\zeta = 3$. (Note that in the case of duct flow, the reflection behaviour is just the opposite, so that upon reflection at a rigid wall,

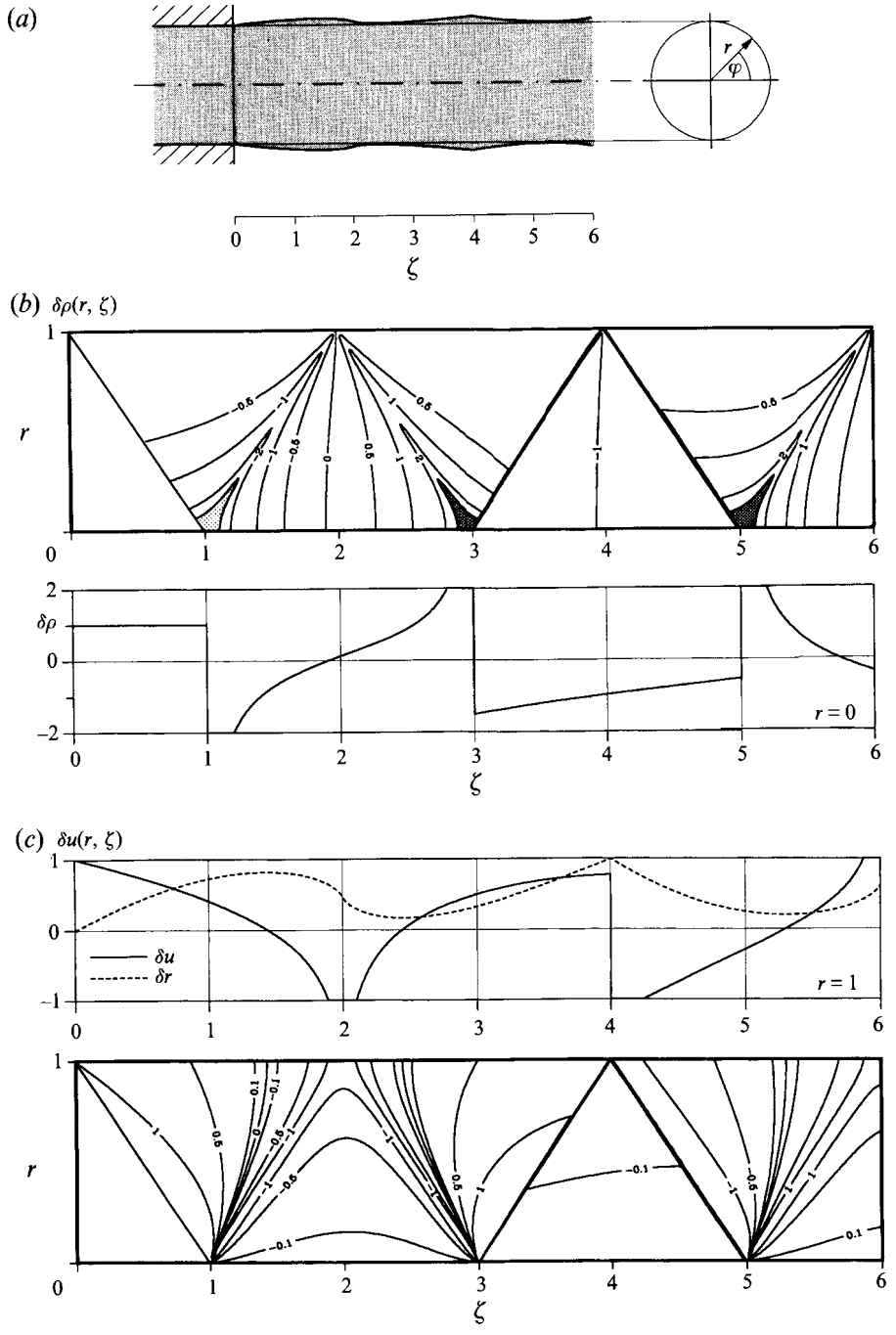

FIGURE 4. Underexpanded axisymmetric free jet (Pack's solution). (*a*) Problem geometry; (*b*) dimensionless density perturbation $\delta\rho(r,\zeta)$ inside the jet (top) and on the jet axis (bottom); (*c*) dimensionless perturbation $\delta u(r,\zeta)$ of radial velocity at the jet boundary (top) and inside the jet (bottom). Dashed curve represents distortion of boundary streamline.

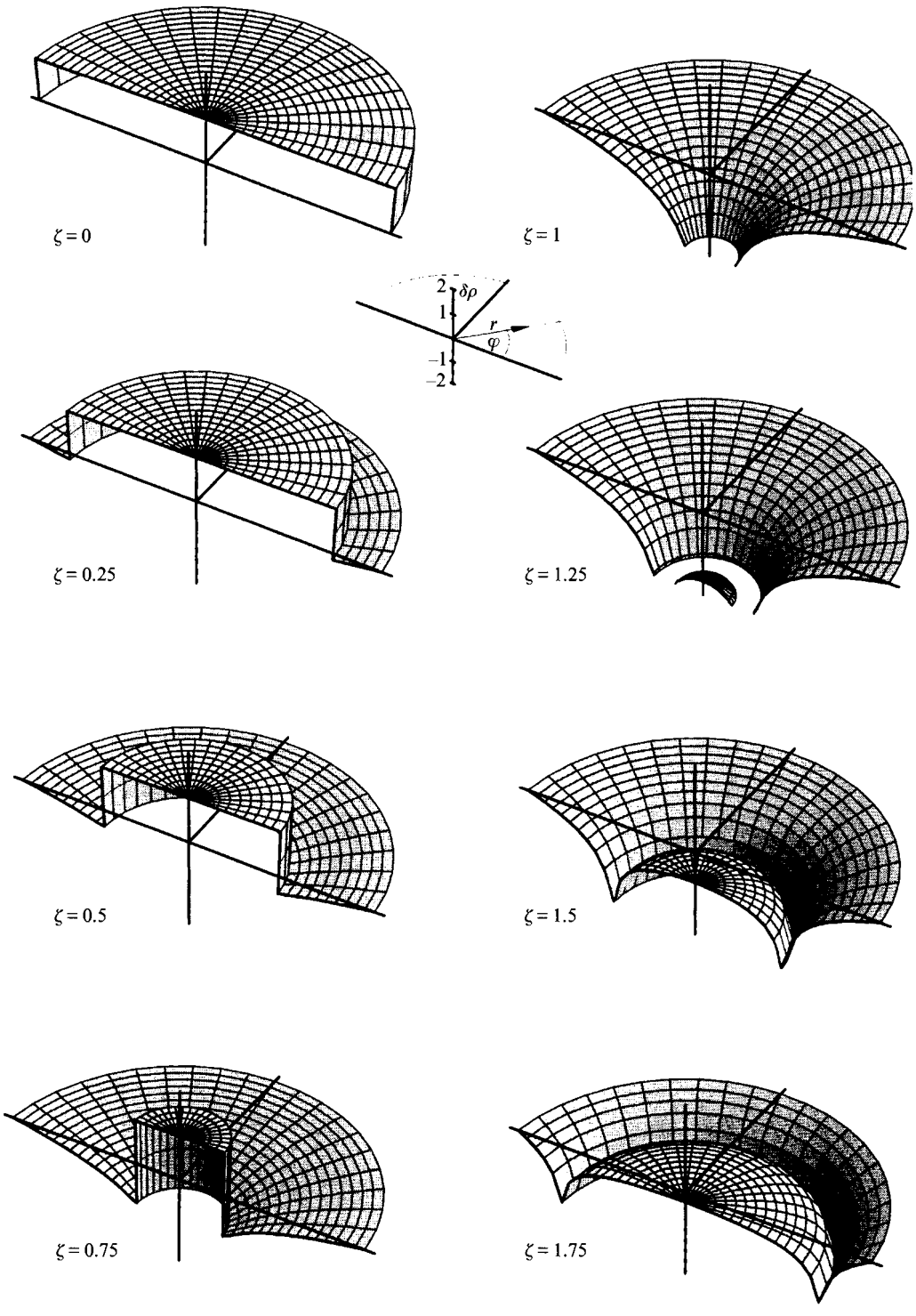

FIGURE 5. Underexpanded axisymmetric free jet (Pack's solution). Surface plots of the dimensionless density perturbation $\delta\rho(r,\zeta)$ in the semicircle $0 \leqslant r \leqslant 1$, $0 \leqslant \varphi \leqslant \pi$ at various locations $\zeta = const.$

an identical low-density region would have been formed.) Now, in full qualitative agreement with the asymptotic propagation laws, the wave is again transformed into its initial discontinuous compression–expansion shape, and after reflection at the boundary at $\zeta = 4$, the whole process is qualitatively repeated with opposite sign (i.e. with a *high*-density region at $r = 0$, $\zeta = 5$ and a *low*-density region at $r = 0$, $\zeta = 7$), so that after reflection at $r = 1$, $\zeta = 8$, the whole cycle starts again. However, as in the case of duct flow, the wave pattern is never strictly periodic because of the incommensurable eigenvalues β_{0n}.

The case $m = 1$ of (5.2), which represents the most simple three-dimensional analogy to Pack's solution, corresponds to a free jet emerging in parallel flow with the pressure distribution across the nozzle exit cross-section having the shape of an oblique disk (as shown in figure 7 for the density distribution at $\zeta = 0$). Figure 6(*a*) shows the problem geometry in the axial cross-section $\varphi = 0, \pi$ while figures 6(*b*) and 6(*c*) present the dimensionless perturbations of density, radial velocity and both axis and streamline distortion in the half-plane $\varphi = 0$ in the same manner as in figure 4. Also, additional surface plots of the dimensionless density perturbation are presented in figure 7 for various locations $\zeta = const.$ Similar to the axisymmetric jet, the discontinuity of pressure at the nozzle edge $r = 1$, $\zeta = 0$ leads to discontinuous waves propagating into the inner portions of the jet, which however are of varying sign and magnitude for different azimuthal angles. Inside the leading Mach cone, the density distribution remains undisturbed, but a linearly increasing radial velocity perturbation (and a corresponding azimuthal component) is induced in the direction of the density gradient. Close to the axis radial focusing occurs as in the axisymmetric case to produce regions of extreme density values close to the axis in the vicinity of $\zeta = 1$, and upon crossing the axis the perturbations are transformed from the discontinuous into the logarithmic type. Hence, the whole physical mechanisms work as in the axisymmetric case with the only difference consisting in the asymmetry and the fact that the axis remains undisturbed since all perturbations cancel out there. Similar results are also to be expected for $m > 1$, so that these cases do not merit a detailed discussion.

6 Comparison with experiment

6.1. *Mach–Zehnder interferograms*

As in the case of duct flow, the existence of singularities has cast considerable doubt on the validity of linear potential theory. For example, Ward (1955) noted that 'the validity of the linearized solution on and near the characteristics $\zeta \pm r = 1, 3, 5 \ldots$ is doubtful' and that 'it is not possible to say whether or not the linearized solution is a valid continuation through $\zeta - r = 1$ and subsequent singularities'. The first attempt at experimental verification is obviously due to Grabitz *et al.* (1979), who calculated theoretical Mach–Zehnder interferograms by numerical integration of the density field provided by Pack's solution and compared them with experimental images. However, the accuracy and spatial resolution of their numerical integration is rather low and the experimental images are strongly disturbed by turbulent fluctuations in the free shear layer. Consequently, while their results indicate that linear potential theory might be adequate to describe the real flow field at least in the portions close to the nozzle orifice, there is still considerable uncertainty about its validity throughout the field. It thus appears appropriate to repeat their comparison using more advanced experimental techniques and a more accurate theoretical treatment.

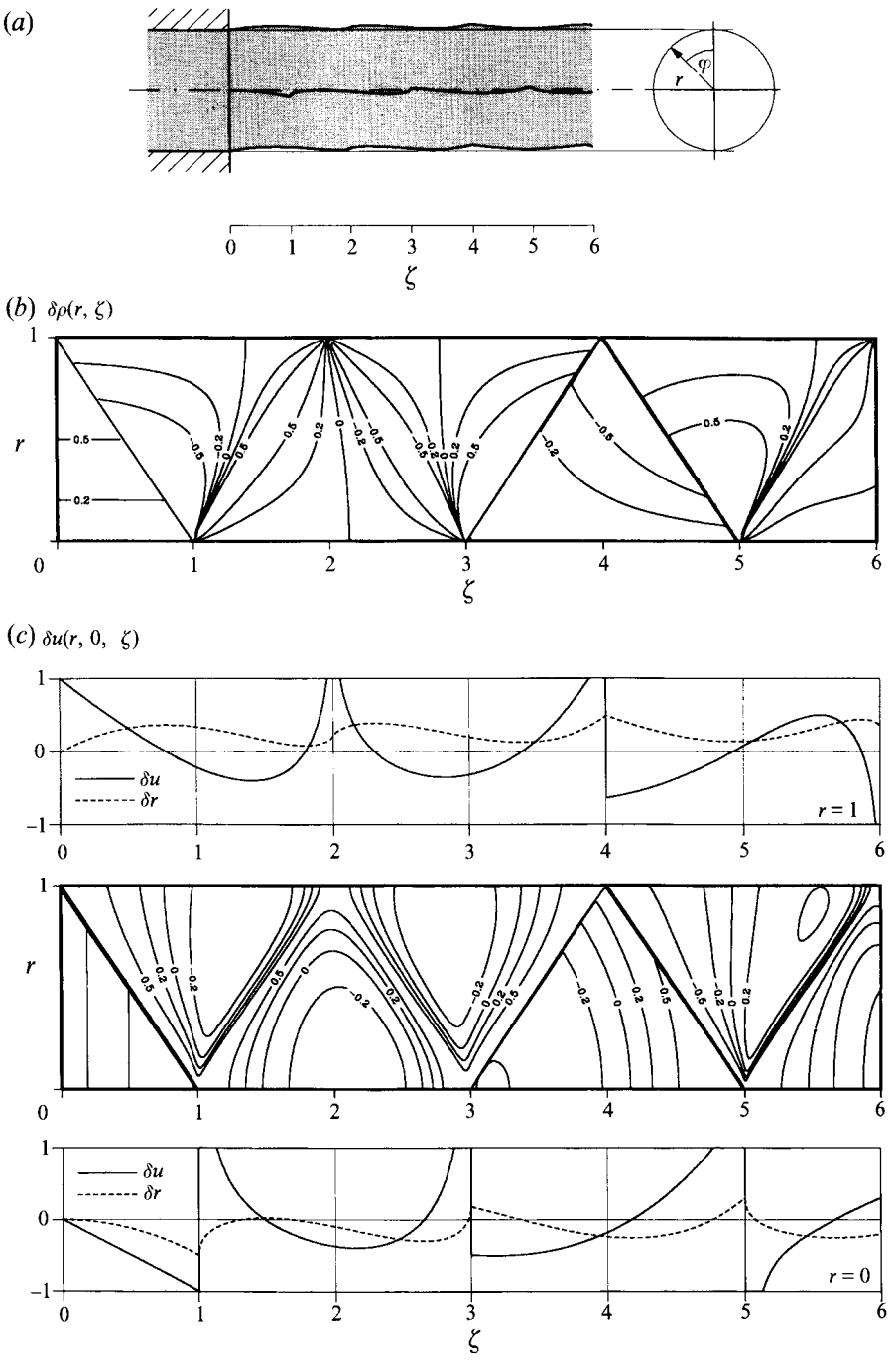

FIGURE 6. Non-axisymmetric free jet emerging with oblique pressure distribution. (*a*) Problem geometry; (*b*) dimensionless density perturbation $\delta\rho(r,\zeta)$ inside the jet; (*c*) dimensionless perturbation $\delta u(r,\zeta)$ of radial velocity at the jet boundary (top), inside the jet (middle) and on the jet axis (bottom). Dashed curves represent distortions of boundary and axis streamlines.

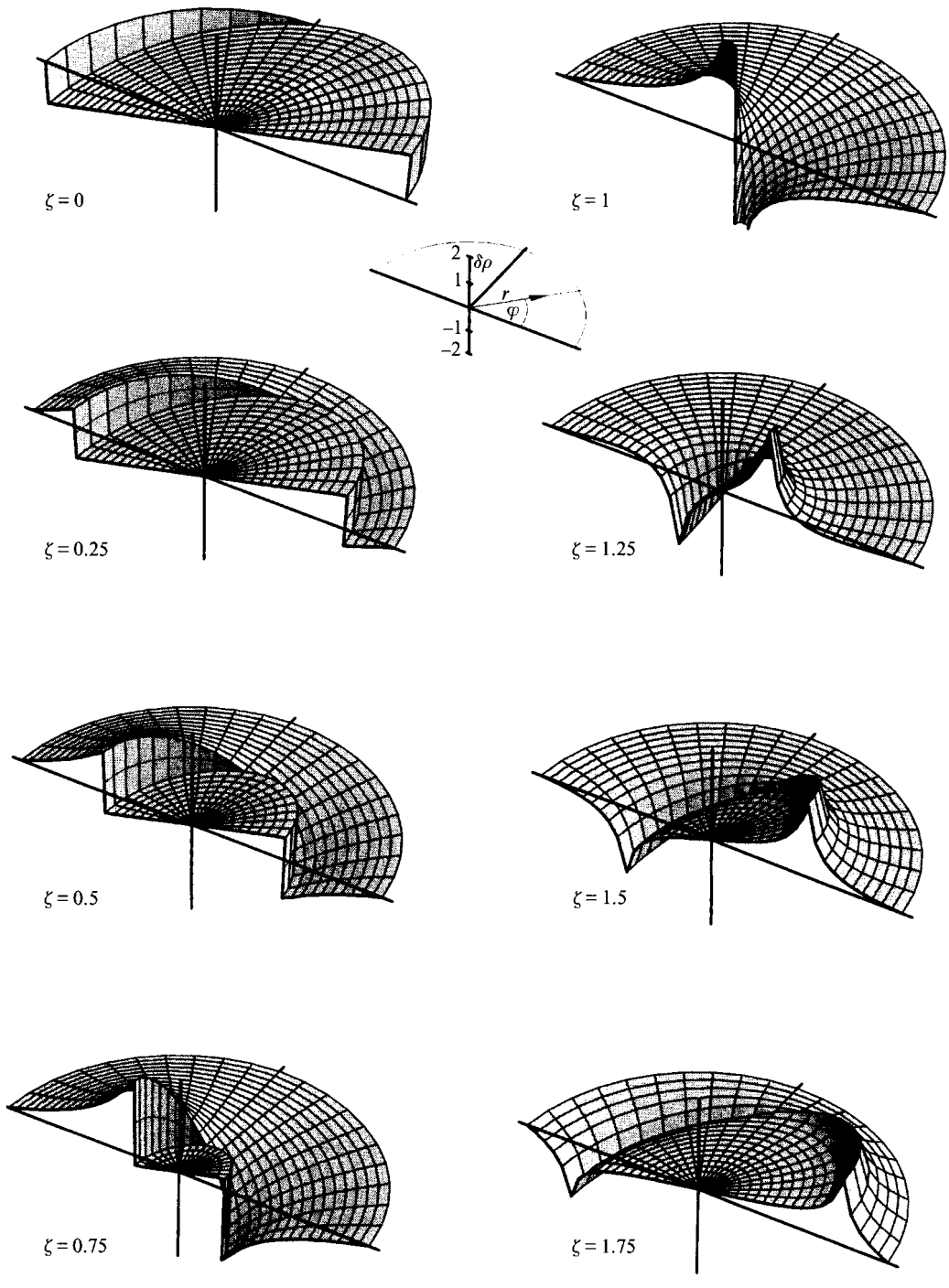

FIGURE 7. Non-axisymmetric free jet emerging with oblique pressure distribution. Surface plots of the dimensionless density perturbation $\delta\rho(r,\zeta)$ in the semicircle $0 \leqslant r \leqslant 1$, $0 \leqslant \varphi \leqslant \pi$ at various locations $\zeta = const.$

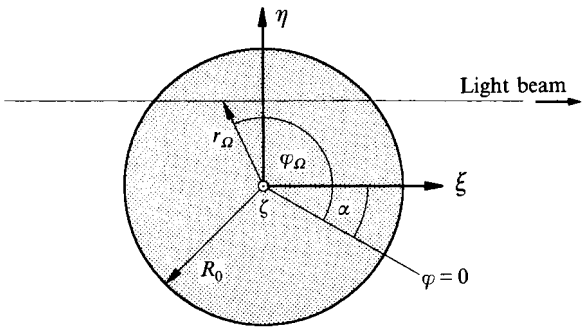

FIGURE 8. Geometry for a straight light beam passing through a cylindrical free jet.

The Mach–Zehnder interferometer is one of the classical instruments of experimental fluid mechanics, which utilizes the variation of the index of refraction of a gas with its density. A parallel monochromatic light beam is split into two coherent beams, one of which passes through the test section, while the other (reference beam) bypasses the test section. When passing through the test section, the first light beam in general suffers a phase shift Δ with respect to the reference beam due to different densities along their paths, so that upon recombination on the interferometer screen, the two beams are no longer in phase:

$$\frac{\Delta}{2\pi} = \frac{n_\infty - 1}{\lambda_0} \int_\Omega \left(\frac{\rho}{\rho_\infty} - 1 \right) \mathrm{d}\omega, \tag{6.1}$$

where λ_0 is the vacuum wavelength of the monochromatic light source, ρ_∞ and n_∞ denote the density and index of refraction of the surrounding medium respectively, and ρ is the variable density inside the test section. The integration variable ω denotes the spatial coordinate in the direction of the light beam and the integral has to be taken over the total length of the light path Ω inside the test section (cf. Goldstein 1983). In deriving (6.1), it has been assumed that the interferometer is operated with infinite fringe setting, which means essentially that the geometrical paths of the reference and test beams have equal lengths.

Thus, constructive or destructive interference can occur depending on the magnitude of the phase shift Δ. The intensity I of the recombined light beam is the quantity observed visually or measured by a photographic device. From elementary wave optics (cf. Goldstein 1983), it can be derived that

$$I = I_0 \cos^2 \Delta/2 \tag{6.2}$$

with I_0 being the peak intensity. It is obvious from (6.2) that if $\Delta/2\pi$ is an integer, the corresponding region on the screen will exhibit maximum brightness, while if $\Delta/2\pi$ is a half-integer, the field will be completely dark. Thus the screen image will consist of a series of bright and dark regions (fringes), each one representative of a specific value of $\Delta/2\pi$ and differing in magnitude from the adjacent fringe of the same intensity by an increment of unity.

In order to calculate theoretical Mach–Zehnder interferograms of cylindrical supersonic free jets, we have to specify (6.1) to the geometry shown in figure 8. Suppose that the test beam is passing through a certain cross-section $\zeta = const.$ of a cylindrical jet (radius R_0) parallel to the ξ-axis at a vertical distance η from the centreline (both coordinates ξ and η are normalized with R_0). The density ρ inside the jet is assumed to be given in the form (2.3*b*) as a function of the polar coordinates r and φ at any

location $\zeta = const.$ The relative position of the test beam with respect to the flow is expressed by the view angle α between the straight line $\varphi = 0$ and the ξ-axis. In order to perform the spatial integration (6.1), we now have to express the polar coordinates r_Ω, φ_Ω of the geometric light path in terms of the Cartesian coordinates ξ, η. From elementary geometric considerations, we obtain

$$r_\Omega = (\xi^2 + \eta^2)^{1/2}, \tag{6.3a}$$

$$\varphi_\Omega = \arctan \frac{\xi \sin\alpha + \eta \cos\alpha}{\xi \cos\alpha - \eta \sin\alpha} \tag{6.3b}$$

and thus, by (2.3*b*), the phase shift (6.1) can be written as

$$\frac{\Delta}{2\pi} = 2(n_\infty - 1)\frac{R_0}{\lambda_0}\left[\left(\frac{\rho_0}{\rho_\infty} - 1\right)(1-\eta^2)^{1/2} - \frac{M_0^2}{(M_0^2-1)^{1/2}}\frac{\rho_0}{\rho_\infty}\frac{1}{2}\int_{-(1-\eta^2)^{1/2}}^{+(1-\eta^2)^{1/2}} \frac{\partial\phi}{\partial\zeta}\Big|_{r_\Omega,\varphi_\Omega,\zeta} \mathrm{d}\xi\right]. \tag{6.4}$$

The calculation of the integral on the right-hand side of (6.4) is thus in general reduced to the termwise integration of the infinite series obtained by termwise differentiation of the velocity potential (2.7) with respect to ζ. In a recent paper by Dillmann (1994*b*), it is shown that the above integration can be performed analytically. For the most general case of the velocity potential (2.7), the following infinite double series is obtained† :

$$\frac{1}{2}\int_{-(1-\eta^2)^{1/2}}^{+(1-\eta^2)^{1/2}} \frac{\partial\phi}{\partial\zeta}\Big|_{r_\Omega,\varphi_\Omega,\zeta} \mathrm{d}\xi = \sum_{m=0}^{\infty}\sum_{n=1}^{\infty} \Theta_m(\beta_{mn}, \eta)\left[\frac{A'_{mn}}{\beta_{mn}}\cos m(\alpha + \tfrac{1}{2}\pi) + \frac{B'_{mn}}{\beta_{mn}}\sin m(\alpha + \tfrac{1}{2}\pi)\right] \tag{6.5}$$

where primes denote differentiation with respect to ζ and $\Theta_m(\lambda, \eta)$ denotes a universal function being given by a double Neumann series (Dillmann 1994*b*):

$$\Theta_m(\lambda,\eta) = 2\sum_{k=0}^{\infty} J_{2k+1}(\lambda(1-\eta^2)^{1/2}) \sum_{j=-k}^{+k}(-1)^j J_{m+2j}(\lambda\eta), \qquad \lambda \geqslant 0, \quad -1 \leqslant \eta \leqslant +1, \tag{6.6}$$

which converges uniformly in its domain of definition and can be used for the numerical computation of $\Theta_m(\lambda, \eta)$. For large values of its first argument λ, $\Theta_m(\lambda, \eta)$ admits the asymptotic expansion (T_m denotes the Chebyshev polynomial of the first kind and order m)

$$\Theta_m(\lambda,\eta) \sim \cos(\lambda\eta - \tfrac{1}{2}m\pi) + \frac{T_m(\eta)}{(1-\eta^2)^{1/2}}\left(\frac{2}{\pi\lambda}\right)^{1/2}\cos(\lambda - \tfrac{1}{2}m\pi - \tfrac{3}{4}\pi) + O(1/\lambda), \qquad -1 < \eta < +1 \tag{6.7}$$

which shows that for $\lambda \to \infty$, $\Theta_m(\lambda, \eta)$ represents a bounded continuous function with an increasing number of oscillations in $-1 < \eta < +1$ for increasing λ. Hence, by means of (6.4)–(6.6), it is in general possible to express the phase shift Δ as an infinite series in terms of $\Theta_m(\beta_{mn}, \eta)$ with its coefficients being directly determined from the velocity potential $\phi(r, \varphi, \zeta)$.

† In the original paper, a somewhat different notation has been used.

For the special case of the velocity potential (5.2) discussed in § 5, we obtain from (6.4) and (6.5)

$$\frac{\Delta}{2\pi} = 2(n_\infty - 1)\frac{R_0}{\lambda_0}\left[\left(\frac{\rho_0}{\rho_\infty} - 1\right)(1-\eta^2)^{1/2} + \frac{\rho_0}{\rho_\infty}\frac{\Delta p}{\kappa p_0}\,\Xi_m(\eta,\zeta)\cos m(\alpha+\tfrac{1}{2}\pi)\right] \quad (6.8a)$$

where $\Xi_m(\eta,\zeta)$ denotes the infinite series

$$\Xi_m(\eta,\zeta) := \sum_{n=1}^{\infty} \frac{2\,\Theta_m(\beta_{mn},\eta)\cos\beta_{mn}\zeta}{\beta_{mn}^2\,J_{m+1}(\beta_{mn})}, \quad (6.8b)$$

which by (3.4), (3.14c) and (6.7), can be shown to converge uniformly and thus to represent a bounded continuous function throughout the field.

Hence, we are now able to calculate theoretical Mach–Zehnder fringe patterns for the free jets discussed in § 5 by simply substituting (6.8) into (6.2). Since (6.8b) represents an integral average of the dimensionless density perturbation (5.4a), a similar spatial structure and cellular pattern of the theoretical interferograms can be expected. By the same methods as used in § 3 and the Appendix to discuss the singular behaviour of $S_m(r,\zeta)$, it can be shown that the first derivatives of $\Xi_m(\eta,\zeta)$ exhibit discontinuities at $\eta \pm \zeta = 2k+1$ (k integer), which are due to the first term of the asymptotic expansion (6.7) and correspond to the projection of the envelope of the leading characteristic surface. Furthermore, additional vertical singularities of the ζ-derivative occur at even integer values of ζ due to the second term of (6.7); in particular, these are logarithmic singularities at $\zeta = 2+4k$ and discontinuities at $\zeta = 4k$ (k integer). Obviously, these singularities are the projections of the base circles of Mach cones, i.e. they indicate the locations where a discontinuity or logarithmic singularity of the internal flow field hits the jet boundary and is reflected back towards the axis. Figure 9(a) presents the complete singularity pattern in the (η,ζ)-plane, while figure 9(b) shows a contour plot of $\Xi_m(\eta,\zeta)$ for the axisymmetric case $m = 0$. Both figures clearly illustrate the pronounced cellular structure of the flow field. The analytical representation (6.8) allows calculations of almost arbitrary spatial resolution and thus theoretical images of nearly photographical quality, which can be compared with corresponding experimental images.

The axisymmetric case $m = 0$ of (5.2), i.e. the solution of Pack, can be physically realized by a parallel-flow Laval nozzle being operated at slightly off-design conditions. Corresponding free jet experiments have been performed at the Max-Planck-Institut für Strömungsforschung in Göttingen, where an appropriate experimental setup was readily available. A slender Laval nozzle was designed with the method of characteristics to produce an ideally expanded uniform parallel flow of Mach number 1.6 at its exit cross-section. The characteristic diameters were 15 mm at the nozzle throat and $R_0 = 16.95$ mm in the exit cross-section; the axial distance between throat and orifice was 67.35 mm. The nozzle was connected via a conduit with a commercial dry air supply system consisting of a compressor, a dehumidifier and a receiver with a capacity of 2 m^3 and a maximum storage pressure of 1.4 MPa. A manually operated control valve in the air supply conduit allowed the throttling of the reservoir pressure to a desired value, which could be read off from an analog manometer. The nozzle exhausted to atmospheric pressure; the free jet emerging from the orifice was observed with a Mach–Zehnder interferometer operated in infinite fringe setting with a field of view of about $2\frac{1}{2}$ nozzle diameters. Behind the control valve, a pressure sensor was installed, whose output signal was electronically compared with a preadjusted threshold to trigger an electronic image aquisition system consisting of a CCD cam-

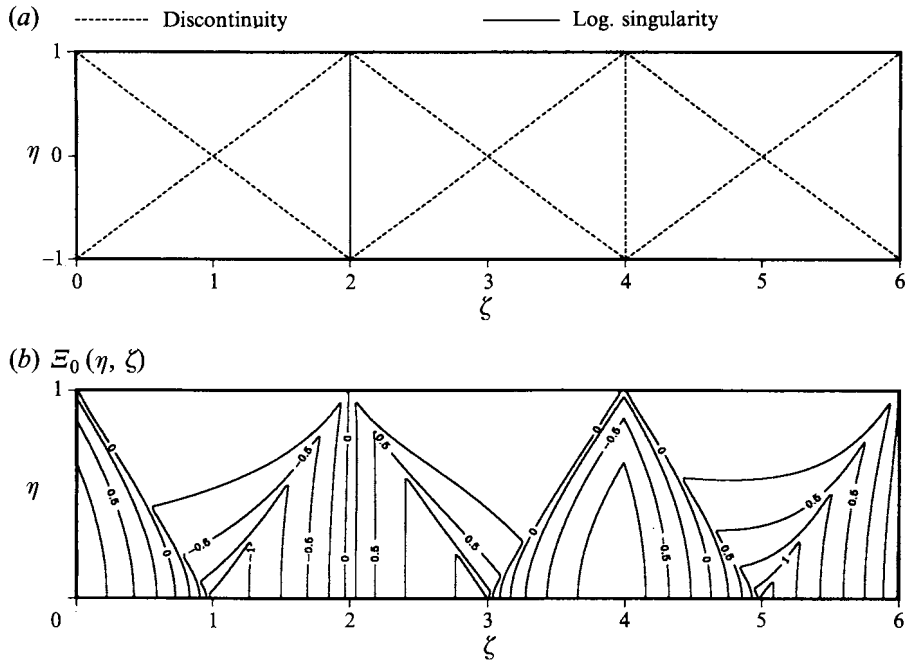

FIGURE 9. The phase shift series $\Xi_m(\eta,\zeta)$ for the axisymmetric case $m = 0$. (*a*) Singularity pattern of the first derivatives in the (η,ζ)-plane; (*b*) contour plot of $\Xi_0(\eta,\zeta)$ for $0 \leqslant \eta \leqslant +1$, $0 \leqslant \zeta \leqslant 6$.

era (resolution 512×512 pixels), a synchronized stroboscope equipped with a pulsed light-emitting diode ($\lambda_0 = 660$ nm), and a microcomputer equipped with a frame grabber. When the control valve was opened and the pressure threshold was reached, the image aquisition system took up to four successive snapshot interferograms with an exposure time of 1 μs in a time distance of 40 ms, which were then stored on the microcomputer for further processing. The time distance between the single snapshots proved to be short enough to ensure steady state efflux conditions for a complete series of four successive pictures.

In order to eliminate the turbulent fluctuations in the free shear layer, time-averaged Mach–Zehnder interferograms were then computed using software developed at the Max-Planck-Institut für Strömungsforschung, which has been described in detail by Bartels-Lehnhoff *et al.* (1993). In a first step, the fringes of each digitized experimental snapshot were extracted by a semi-automatic algorithm and approximated by polygons. The resulting polygons were then numbered according to their order of interference by using a graphical editor. The complete field of the order of interference, i.e. the phase shift Δ, was then obtained by interpolation between the numbered polygons using the intensity I in the original interferogram. Thus, for each experimental snapshot, a high-resolution field of the phase shift Δ was obtained. The time-averaged field was then obtained by computing the pointwise arithmetic mean of eight snapshot fields. Finally, the time-averaged phase shift Δ was substituted into equation (6.2) to yield the time-averaged interferogram.

Examples of an underexpanded and an overexpanded axisymmetric supersonic free jet are presented on the left- and right-hand sides of figure 10, respectively. On each side, photograph (*a*) shows an experimental snapshot, photograph (*b*) the time-averaged interferogram obtained from eight experimental snapshots, and photograph

(*c*) shows the corresponding theoretical interferogram computed from (6.2) and (6.8) for $m = 0$ with $n_\infty - 1 = 2.719 \times 10^{-4}$, $R_0 = 16.95$ mm and $\lambda_0 = 660$ nm. The corresponding values of the parameters ρ_0/ρ_∞, $\Delta p/\kappa p_0$ and M_0 were determined from the time-averaged interferograms by least-squares fitting of the experimental and theoretical fringes in the nozzle exit cross-section $\zeta = 0$ and on the jet axis $\eta = 0$. While in the experimental snapshots, only the portions close to to the nozzle orifice are clearly recognizable and the structures further downstream are strongly disturbed by turbulent fluctuations, the time-averaging process has almost completely eliminated any random perturbations so that only the steady state component of the free jet flow field remains. The agreement between the time-averaged and the theoretical interferograms is striking; the geometric shape and location of all fringes are almost identical and deviations only occur in minor details. At the jet boundary, the theoretical fringe density is somewhat higher and the fringes are thinner than in experiment, which can be explained by the fact that, theoretically, a rectangular initial pressure distribution and an ideal separating vortex sheet have been assumed, while in reality, steep gradients at the boundary are smoothed by boundary layer effects. Nevertheless, the excellent overall agreement between theory and experiment removes any doubt that linear potential theory is adequate to describe supersonic free jet flow even close to the singularities and that it is indeed a valid continuation through $\zeta - r = 1$ and subsequent singularities.

6.2. *The wavelength of an axisymmetric free jet*

The cellular, almost periodic structure of supersonic free jets represents their most prominent feature. Commonly, the spatial distance between two subsequent shock reflections at the jet boundary is called the 'wavelength' of a free jet, the resulting 'diamond pattern' being clearly visible in schlieren pictures and shadowgraphs. A number of theoretical investigations has been made with the object of predicting free jet wavelengths, the most prominent of these being due to Pack (1950). Following an interpretation by Prandtl (1904), Pack assumed that the end of the first shock cell coincides with the first minimum of the jet boundary, as this is the case for plane jets. As can be seen from the dashed line in figure 4(*c*), the first minimum is placed in the vicinity of $\zeta = 2.44$ and consequently Pack obtained the following formula for the wavelength L of the first shock cell:

$$L = 1.22\, D\, (M_0^2 - 1)^{1/2} \tag{6.9}$$

where $D = 2R_0$ denotes the orifice diameter of the nozzle. However, Pack's formula is inconsistent. From figure 4 it is clearly obvious that the first minimum of the jet boundary is not associated with any discrete event in the jet flow pattern, whose cellular structure is determined by the singularities transversing the jet once in a distance $\Delta\zeta = 2$. Also, from the considerations in the previous section, there is no doubt that the diamond pattern visible in schlieren pictures and shadowgraphs is associated with the singularity pattern of the phase shift Δ, which according to figure 9, exhibits the same characteristic length. (Note that in schlieren pictures and shadowgraphs, the first and second derivatives of Δ are visualized, respectively.) Therefore, the correct formula for the wavelength is

$$L = D\, (M_0^2 - 1)^{1/2}, \tag{6.10}$$

which, of course, differs from Pack's result and is identical with the corresponding length in a plane free jet.

In his pioneering experimental study, Emden (1899) determined the wavelengths

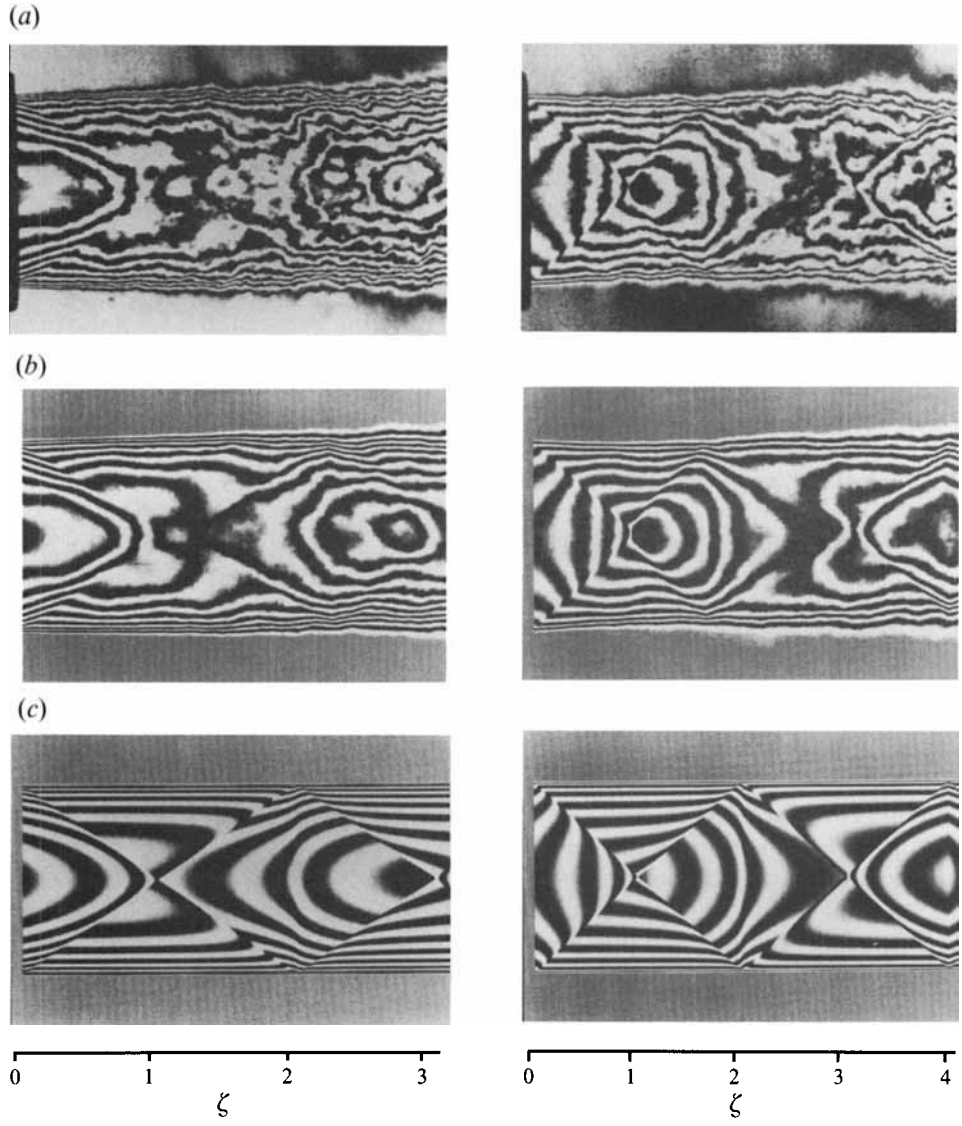

FIGURE 10. Comparison between theory and experiment for the axisymmetric case $m = 0$ of the velocity potential (5.2) (Pack's solution). Photographs on the left- and right-hand sides correspond to an underexpanded and overexpanded free jet, respectively. Theoretical parameters are $\rho_0/\rho_\infty = 1.497$, $\Delta p/\kappa p_0 = +0.073$ and $M_0 = 1.75$ for the underexpanded and $\rho_0/\rho_\infty = 1.370$, $\Delta p/\kappa p_0 = -0.092$ and $M_0 = 1.48$ for the overexpanded jet. (*a*) Experimental snapshot Mach–Zehnder interferogram; (*b*) time-averaged Mach–Zehnder interferogram obtained from eight snapshot pictures; (*c*) theoretical Mach–Zehnder interferogram computed from (6.2) and (6.8).

of supersonic free jets of air, carbon dioxide and hydrogen, which were obtained by the discharge of a reservoir through a number of nozzles of different shapes but convergent to the orifice. By careful evaluation of more than 300 shadowgraphs, he found that the wavelength L could with great accuracy be expressed by the empirical fit

$$L = 0.88\, D \left(\frac{p_R}{p_0} - 1.9\right)^{1/2}, \tag{6.11}$$

i.e. L depends on the ratio of reservoir pressure p_R to ambient pressure p_0, which in Emden's experiments varied from 1.9 up to 20. Note that Emden found (6.11) to hold for *both* axisymmetric and plane jets, which is also an indication that (6.10) and not (6.9) is the correct expression for the wavelength. Pack compared his formula with Emden's empirical fit by expressing the Mach number at ideal expansion M_0 in terms of the pressure ratio p_R/p_0 via Bernoulli's equation

$$M_0^2 = \frac{2}{\kappa-1}\left(\left(\frac{p_R}{p_0}\right)^{\frac{\kappa-1}{\kappa}} - 1\right), \tag{6.12}$$

which however has the disadvantage that the resulting expression does not depend on the pressure ratio in the nozzle orifice, i.e. on the crucial quantity deciding whether or not linear theory can be applied. Therefore, it appears more appropriate to express the right-hand sides of (6.9), (6.10) and (6.11) in terms of the efflux Mach number M_N (which, in general, differs from the ideal expansion Mach number M_0) and the pressure perturbation Δp in the orifice. Again, from Bernoulli's equation, we obtain

$$\frac{p_R}{p_0} = \left(1 + \frac{\kappa-1}{2} M_N^2\right)^{\frac{\kappa}{\kappa-1}} \left(\frac{\Delta p}{p_0} + 1\right), \tag{6.13a}$$

$$M_0^2 = \frac{2}{\kappa-1}\left[\left(1 + \frac{\kappa-1}{2} M_N^2\right)\left(\frac{\Delta p}{p_0} + 1\right)^{\frac{\kappa-1}{\kappa}} - 1\right], \tag{6.13b}$$

which have to be substituted into (6.9), (6.10) and (6.11) to yield the wavelength L/D as a function of nozzle exit Mach number M_N and dimensionless pressure perturbation $\Delta p/p_0$.

Figure 11 shows a comparison of the dimensionless wavelengths L/D for Pack's formula (6.9), equation (6.10) and Emden's empirical fit (6.11) for $M_N = 1$ (i.e. sonic conditions at the nozzle exit), $\kappa = 1.4$ and $0 \leqslant \Delta p/p_0 \leqslant 1$. The agreement between Emden's formula and equation (6.10) is remarkable, whereas the predictions of (6.9) are clearly too high. Obviously, the correct formula for the wavelength of a supersonic free jet is (6.10) and not (6.9), and it seems that the capability of linear theory to predict wavelengths reaches far beyond the limit $\Delta p/p_0 \ll 1$ where it can give an adequate description of the internal flow field.

7 Summary and conclusions

In this paper, the methods developed in Part 1 for supersonic duct flow have been extended to free jet flow. By decomposition of the flow into an ideally expanded homogeneous parallel flow and small irrotational perturbations, the mathematical formulation in § 2 leads to an initial-boundary value problem for the wave equation (2.1), which differs from that obtained for duct flow only by the boundary condition (2.5) prescribing the velocity potential at $r = 1$ instead of its normal derivative. The general solution arises in the form of the infinite double series (2.7), which can be interpreted as a harmonic Fourier series in the azimuthal angle φ, with each coefficient being itself an infinite Fourier–Bessel series of the first kind. The coefficients of the Fourier–Bessel series obey the well-known ordinary differential equation (2.11) of a mass–spring system with constant exciting force and thus the problem of cylindrical supersonic free jet flow has been solved for arbitrary axisymmetric and non-axisymmetric efflux conditions at the nozzle orifice.

In § 3, it has been shown that supersonic free jet flow exhibits essentially the

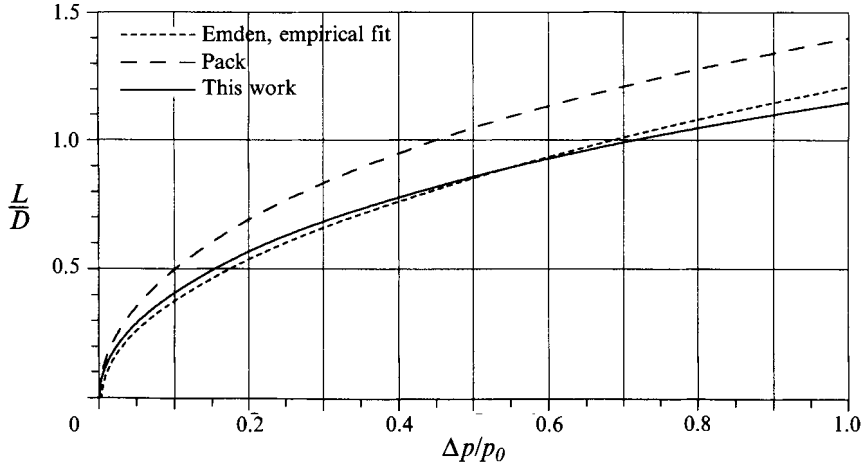

FIGURE 11. The wavelength L/D of a supersonic free jet at sonic exit conditions ($M_N = 1$) according to Pack's formula (6.9), equation (6.10) and Emden's empirical fit (6.11). Relations (6.13) have been used to express L/D in terms of the pressure perturbation $\Delta p/p_0$.

same singularities as the flow in ducts, which determine the cellular structure of the flow pattern and cause non-uniform convergence of the infinite series describing the physical flow variables. This phenomenon arises whenever a discontinuity of pressure at the nozzle edge occurs, and it has been shown that the axial and radial velocity components exhibit jumps at this location which satisfy the Ackeret relation, i.e. the Prandtl–Meyer relation in the linear limit. Thus, as in the case of duct flow, the bending of boundary streamlines gives rise to singularities propagating along the leading characteristic. In order to allow a discussion of singular behaviour and to resolve the numerical problems associated with non-uniform convergence, the method of Kummer's series transformation, which has also been succesfully applied in Part 1, has been extended to the present case.

For a qualitative understanding of the resulting flow fields, the asymptotic laws governing the propagation of small perturbations along downstream characteristics have been derived in § 4. While upon transmission through the axis, a perturbation of a flow variable (except radial velocity) suffers an asymptotic phase shift of $\pi/2$ and increases as $r^{-1/2}$ as the axis is approached, it suffers a phase shift of π when being reflected at the jet boundary. (For a radial velocity perturbation, the phase shift is $-\pi/2$ upon transmission through the axis, whereas it is reflected unchanged at the wall.) Thus, while the transmission behaviour on the axis is the same as in the case of duct flow, it is just opposite at the free jet boundary.

Two elementary cases of axisymmetric and non-axisymmetric supersonic free jet flow have been extensively discussed in § 5, along with Pack's classical solution for the axisymmetric jet with constant pressure perturbation at the nozzle orifice, for which no complete evaluation has been available in the literature although the formal solution has been known since 1950. The resulting flow fields exhibit a similar structure to the case of duct flow, but the spatial arrangement of compression and expansion regions is different due to the opposite reflection behaviour at the jet boundary.

The singular nature of the solutions provided by linear potential theory has raised considerable doubt in the literature about its ability to describe the real flow field. For

the special case of the axisymmetric free jet described by Pack's solution, simple free jet experiments have been performed. Time-averaged Mach–Zehnder interferograms have been computed from experimental snapshot pictures, and have been compared with theoretical images obtained by analytical integration of the density field for an underexpanded and an overexpanded free jet, respectively. The excellent agreement shows that linear theory is adequate to describe the real flow fields, even close to the singularities and also far downstream of the nozzle orifice.

Furthermore, the wavelength predicted by linear theory has been examined, since this question is still subject to controversy in literature (cf. Carpenter 1978; Powell 1992). It has been shown that the formula of Pack (1950), which is still widely accepted, is based on an incorrect interpretation of the wavelength as the location of the first minimum of the jet contour, which however is not associated with the characteristic length of the intersecting shock pattern inside the jet. The correct formula (6.10), which is identical with the one obtained for plane jets, has been shown to be in excellent agreement with experiment, whereas the predictions of Pack's formula are about 20% too high.

Thus, linear potential theory has been shown to describe real free jet flow in an adequate manner. Since the case of duct flow treated in Part 1 is based on essentially the same equations and differs from the present problem only by the boundary condition, it appears very likely that linear potential theory would describe the real flow in quasi-cylindrical ducts with similar success.

Parts of this work have been supported by a habilitation scholarship of the Deutsche Forschungsgemeinschaft, which is gratefully acknowledged. The author is also indebted to his colleagues Mr T. Wetzel and Dr C. Söller at the Max-Planck-Institut für Strömungsforschung for indispensable experimental support and for producing the time-averaged interferograms.

Appendix.

By differentiating the definition (3.7) of $S_m(r,\zeta)$ termwise with respect to r and ζ respectively, and adopting the notation introduced in (3.13), the terms of the corresponding infinite series can be written as

$$s_{mn,r}(r,\zeta) = \frac{2\,J'_m(\beta_{mn}r)\,\sin\beta_{mn}\zeta}{\beta_{mn}\,J_{m+1}(\beta_{mn})}, \tag{A 1a}$$

$$s_{mn,\zeta}(r,\zeta) = \frac{2\,J_m(\beta_{mn}r)\,\cos\beta_{mn}\zeta}{\beta_{mn}\,J_{m+1}(\beta_{mn})}, \tag{A 1b}$$

from which, by substituting the asymptotic expansions (3.14) of the Bessel functions and their zeros, we obtain the following asymptotic expansions valid for large n:

$$s_{mn,r}(r,\zeta) \sim -\frac{1}{r^{1/2}}\left[\frac{\sin\mu_{mn}(r+\zeta-1)}{\mu_{mn}} - \frac{\sin\mu_{mn}(r-\zeta-1)}{\mu_{mn}}\right] + O\left(\frac{1}{n^2}\right), \tag{A 2a}$$

$$s_{mn,\zeta}(r,\zeta) \sim -\frac{1}{r^{1/2}}\left[\frac{\sin\mu_{mn}(r+\zeta-1)}{\mu_{mn}} + \frac{\sin\mu_{mn}(r-\zeta-1)}{\mu_{mn}}\right] + O\left(\frac{1}{n^2}\right), \tag{A 2b}$$

provided that $r > 0$. In the case $r = 0$, r must be put equal to zero *before* introducing the asymptotic expansions (3.14), and we get

$$s_{mn,r}(0,\zeta) \sim \begin{cases} -(\pi/2)^{1/2}\,(-1)^n \dfrac{\sin \mu_{1n}\zeta}{(\mu_{1n})^{1/2}} + O\left(\dfrac{1}{n^{3/2}}\right), & m = 1 \\ 0, & \text{otherwise}, \end{cases} \tag{A 3a}$$

$$s_{mn,\zeta}(0,\zeta) \sim \begin{cases} -(2\pi)^{1/2}\,(-1)^n \dfrac{\cos \mu_{0n}\zeta}{(\mu_{0n})^{1/2}} + O\left(\dfrac{1}{n^{3/2}}\right), & m = 0 \\ 0, & \text{otherwise}, \end{cases} \tag{A 3b}$$

since $J_m(0) = 0$ for all $m \neq 0$ and $J'_m(0) = 0$ for all $m \neq 1$. Obviously, the asymptotic expansions (A 2), (A 3) satisfy (3.11), and thus their leading terms can be used in Kummer's series transformation (3.12) as comparison terms for the derivatives (3.13) of $S_m(r,\zeta)$.

Hence, by introducing the notation

$$\Psi_m(x) = \sum_{n=1}^{\infty} \psi_{mn}(x) = \sum_{n=1}^{\infty} \frac{\sin \mu_{mn} x}{\mu_{mn}}, \tag{A 4a}$$

$$\Omega_0(x) = \sum_{n=1}^{\infty} \omega_{0n}(x) = \sum_{n=1}^{\infty} (-1)^n \frac{\cos \mu_{0n} x}{(\mu_{0n})^{1/2}}, \tag{A 4b}$$

$$\Omega_1(x) = \sum_{n=1}^{\infty} \omega_{1n}(x) = \sum_{n=1}^{\infty} (-1)^n \frac{\sin \mu_{1n} x}{(\mu_{1n})^{1/2}}, \tag{A 4c}$$

we can write the comparison terms $\tilde{s}_{mn,r}(r,\zeta)$, $\tilde{s}_{mn,\zeta}(r,\zeta)$ in the form

$$\tilde{s}_{mn,r}(r,\zeta) = \begin{cases} -r^{-1/2}\,[\psi_{mn}(r+\zeta-1) - \psi_{mn}(r-\zeta-1)], & r > 0 \\ -(\pi/2)^{1/2}\,\omega_{1n}(\zeta), & r = 0,\ m = 1 \\ 0, & \text{otherwise}, \end{cases} \tag{A 5a}$$

$$\tilde{s}_{mn,\zeta}(r,\zeta) = \begin{cases} -r^{-1/2}\,[\psi_{mn}(r+\zeta-1) + \psi_{mn}(r-\zeta-1)], & r > 0 \\ -(2\pi)^{1/2}\,\omega_{0n}(\zeta), & r = 0,\ m = 0 \\ 0, & \text{otherwise}, \end{cases} \tag{A 5b}$$

while the comparison sums $\tilde{S}_{m,r}(r,\zeta)$, $\tilde{S}_{m,\zeta}(r,\zeta)$ can be expressed as

$$\tilde{S}_{m,r}(r,\zeta) = \begin{cases} -r^{-1/2}\,[\Psi_m(r+\zeta-1) - \Psi_m(r-\zeta-1)], & r > 0 \\ -(\pi/2)^{1/2}\,\Omega_1(\zeta), & r = 0,\ m = 1 \\ 0, & \text{otherwise}, \end{cases} \tag{A 6a}$$

$$\tilde{S}_{m,\zeta}(r,\zeta) = \begin{cases} -r^{-1/2}\,[\Psi_m(r+\zeta-1) + \Psi_m(r-\zeta-1)], & r > 0 \\ -(2\pi)^{1/2}\,\Omega_0(\zeta), & r = 0,\ m = 0 \\ 0, & \text{otherwise}, \end{cases} \tag{A 6b}$$

and are thus completely related to the simple Fourier series (A 4), whose closed sums

remain to be determined. As has been shown by Dillmann & Grabitz (1994), this task can be solved by use of Lerch's transcendent function. For the Fourier series (A 4*a*), one obtains

$$\Psi_m(x) = \begin{cases} -\sum_{n=1}^{m/2} \frac{\sin \mu_{0n} x}{\mu_{0n}} + \frac{1}{2} \operatorname{sgn} \sin \pi x/4 + \frac{1}{2\pi} \ln \frac{1-\sin \pi x/4}{1+\sin \pi x/4}, & m \text{ even}, \\ -\sum_{n=0}^{(m-1)/2} \frac{\sin \mu_{1n} x}{\mu_{1n}} + \frac{1}{2} \operatorname{sgn} \sin \pi x/4 - \frac{1}{2\pi} \ln \frac{1-\sin \pi x/4}{1+\sin \pi x/4}, & m \text{ odd}, \end{cases} \tag{A 7}$$

where $\operatorname{sgn} x$ denotes the signum function, which gives $-1,0$ or $+1$ depending on whether x is negative, zero or positive. As is obvious from (A 7), $\Psi_m(x)$ is a periodic function with period 8, which has discontinuities of magnitude 1 at $x = 4k$ due to the signum function and logarithmic poles of alternating sign at $x = 4k+2$ with k being an integer number.

For the two Fourier series (A 4*b*) and (A 4*c*), Dillmann & Grabitz (1994) obtain the analytical sums

$$\Omega_0(x) = \frac{1}{2(2\pi)^{1/2}} \left[Z\left(\frac{7+x}{8}\right) + Z\left(\frac{7-x}{8}\right) - Z\left(\frac{3+x}{8}\right) - Z\left(\frac{3-x}{8}\right) \right] \tag{A 8}$$

$$\Omega_1(x) = \frac{1}{2(2\pi)^{1/2}} \left[Z\left(\frac{7+x}{8}\right) - Z\left(\frac{7-x}{8}\right) - Z\left(\frac{3+x}{8}\right) + Z\left(\frac{3-x}{8}\right) \right] - \frac{2}{(\pi)^{1/2}} \sin \pi x/4, \tag{A 9}$$

where $Z(x)$ denotes a function of period 1, which in $[0,1]$ is identical with the special case $s = \frac{1}{2}$ of Riemann's generalized zeta function $\zeta(s,x)$ (cf. Whittaker & Watson 1927). Tables and computational relations for $\zeta(\frac{1}{2},x)$ have been given by Powell (1952). Since for $x \to 0$, $\zeta(\frac{1}{2},x)$ approaches infinity as $1/x^{1/2}$, $Z(x)$ exhibits the same behaviour whenever its argument is an integer number. Consequently, the functions $\Omega_0(x)$ and $\Omega_1(x)$ are functions of period 8 and exhibit inverse-square-root singularities at $x = 2k+1$, k integer.

Addendum

In Part 1 of this work (Dillmann 1994*a*) there is a factor r missing in the argument of the Bessel function appearing in the *numerator* of the infinite series expressions in equations (5.3) and (5.9). In both cases, $J_0(\beta'_{0n})$ has to be replaced by $J_0(\beta'_{0n} r)$. Furthermore, 'period ω' at the bottom of page 185 (Note on Schlömilch series) should be replaced by 'frequency ω'; and the initial page of Prandtl's paper in the list of references is 599.

REFERENCES

ABRAMOWITZ, M. & STEGUN, I. A. 1972 *Handbook of Mathematical Functions*. Dover.

BARTELS-LEHNHOFF, H.-H., BAUMANN, P. H., BRETTHAUER, B. & MEIER, G. E. A. 1993 Computer aided evaluation of interferograms. *Exps. Fluids* **16**, 46–53.

BLEISTEIN, N. & HANDELSMAN, R. A. 1986 *Asymptotic Expansions of Integrals*. Dover.

CARPENTER, P. W. 1978 A small perturbation theory for supersonic jets. *AIAA Paper* 78–1151.

DILLMANN, A. 1994*a* Linear potential theory of steady internal supersonic flow with quasi-cylindrical geometry. Part 1. Flow in ducts. *J. Fluid Mech.* **281**, 159–191.

DILLMANN, A. 1994*b* On the calculation of theoretical Mach–Zehnder interferograms from the given velocity potential of a cylindrical supersonic free jet. *Acta Mechanica* **104**, 143–157.

DILLMANN, A. & GRABITZ, G. 1994 On a method to evaluate Fourier–Bessel series with poor convergence properties and its application to linearized supersonic free jet flow. *Q. Appl. Maths* (in press).

EMDEN, R. 1899 Über die Ausströmungserscheinungen permanenter Gase. *Ann. Phys. Chem.* **69**, 264–289 and 426–453.

GOLDSTEIN, R. J. 1983 *Fluid Mechanics Measurements*. Hemisphere.

GRABITZ, G. 1975 Analytische Lösung für den stationären rotationssymmetrischen Überschallfreistrahl in linearer Näherung. *Z. Angew. Math. Mech.* **55**, T127–T130.

GRABITZ, G., HILLER, W. J. & MEIER, G. E. A. 1979 Die Dichteverteilung in einem stationären, rotationssymmetrischen Überschallfreistrahl, der gegen schwachen Unter- oder Überdruck austritt. In *Recent Developments in Theoretical and Experimental Fluid Mechanics* (ed. U. Müller, K. G. Roesner & B. Schmidt), pp. 144–156. Springer.

OSWATITSCH, K. 1952 *Theoretische Gasdynamik*. Springer.

PACK, D. C. 1950 A note on Prandtl's formula for the wavelength of a supersonic gas jet. *Qt. J. Mech. Appl. Maths* **3**, 173–181.

POWELL, E. O. 1952 A table of the generalized Riemann zeta function in a particular case. *Qt. J. Mech. Appl. Maths* **5**, 116–123.

POWELL, A. 1992 Physics of standing waves in circular underexpanded jets. *J. Acoust. Soc. Am.* **91**, 2354.

PRANDTL, L. 1904 Über die stationären Wellen in einem Gasstrahl. *Physik. Z.* **5**, 599–601.

RAYLEIGH LORD 1916 On the discharge of gases under high pressures. *Phil. Mag.* (6) **32**, 177-187.

TOLSTOV, G. P. 1976 *Fourier Series*. Dover.

WARD, G. N. 1955 *Linearized Theory of Steady High-Speed Flow*. Cambridge University Press.

WATSON, G. N. 1944 *A Treatise on the Theory of Bessel Functions*. Cambridge University Press.

WHITTAKER, E. T. & WATSON, G. N. 1927 *A Course of Modern Analysis*. Cambridge University Press.